

Subtracted Dispersion Relations for Virtual Compton Scattering off the Proton

Igor Danilkin,¹ Barbara Pasquini,^{2,3} Matteo Ronchi,^{1,2} and Marc Vanderhaeghen¹

¹*Institut für Kernphysik and PRISMA⁺⁺ Cluster of Excellence,
Johannes Gutenberg-Universität, Mainz, D-55099, Germany*

²*Dipartimento di Fisica "A. Volta", Università degli Studi di Pavia, I-27100 Pavia, Italy*

³*Istituto Nazionale di Fisica Nucleare, Sezione di Pavia, I-27100 Pavia, Italy*

(Dated: March 11, 2026)

We present a once-subtracted dispersion relation (DR) formalism for the virtual Compton scattering (VCS) process from threshold up to the $\Delta(1232)$ energy region. The formalism aims at extracting the nucleon's electric and magnetic generalized polarizabilities from the $e^-p \rightarrow e^-\gamma p$ process, in view of the precision goals of the present and near future experiments at Jefferson Lab. The present work improves upon the existing unsubtracted DR formalism in several ways. The required s - and t -channel discontinuities in the subtracted dispersion integrals are obtained in a largely data-driven manner in this energy region. The s -channel dispersive integrals are reconstructed from $\gamma^*p \rightarrow \pi N \rightarrow \gamma p$ using pion photo- and electro-production data, while the t -channel dispersion integrals are evaluated from $\gamma^*\gamma \rightarrow \pi\pi \rightarrow N\bar{N}$ using recent dispersive analyses of both the $\gamma^*\gamma \rightarrow \pi\pi$ and $\pi\pi \rightarrow N\bar{N}$ processes. We compare our results to VCS data and show the sensitivity of the observables to the nucleon's scalar generalized polarizabilities, which enter the present formalism as subtraction constants.

I. INTRODUCTION

The electromagnetic polarizabilities of the nucleon are elementary structure constants that encode its response to slowly varying external electric and magnetic fields, and provide stringent tests of our understanding of low-energy QCD. In real Compton scattering (RCS), the leading scalar polarizabilities (electric α_{E1} and magnetic β_{M1}) and their spin counterparts can be accessed through precision measurements of photon-nucleon scattering; see [1, 2] for the most recent experiments and [3] for the first simultaneous extraction of the six leading-order proton polarizabilities. The extraction of polarizabilities has long served as a benchmark for effective field theory and dispersion-theoretical descriptions of hadron structure; see [4–7] for reviews. The nucleon polarizabilities also enter the hadronic corrections to precision Hydrogen spectroscopy, where the polarizability contribution corresponds to the two-photon exchange process between the lepton and the proton in the Hydrogen atom. These two-photon exchange corrections are currently a dominant source of theoretical uncertainty in the Standard Model prediction of the Lamb shift and Hyperfine splitting of muonic Hydrogen and light muonic atoms; see [8, 9] for recent reviews. An improved understanding of these polarizability corrections is timely and necessary in view of the ongoing spectroscopy experiments, which aim to extract nucleon and nuclear radii with improved precision. Virtual Compton scattering (VCS), in which the incoming real photon is replaced by a space-like virtual photon, extends this program to generalized polarizabilities (GPs) [10, 11]. The GPs, which depend on the photon virtuality Q^2 , allow us to map the spatial distributions of the induced polarization and magnetization densities of the nucleon [12], therefore providing spatially resolved information on the nucleon's response to external electromagnetic fields. A substantial experi-

mental program has established VCS as a precision tool, with measurements performed at the Mainz Microtron (MAMI) [13–19], MIT-Bates [20, 21], and Jefferson Lab (JLab) [22–24]; see [4, 25, 26] for reviews.

Dispersion relations (DRs) provide a particularly powerful tool for extracting polarizabilities and GPs from RCS and VCS data, respectively, because they connect these low-energy structure parameters to the excitation spectrum of the nucleon and to photo- and electro-production data through analyticity and unitarity. Their application to the Compton process has a long history, dating back to the works of Gell-Mann, Goldberger, and Thirring [27] and Goldberger [28], who derived DRs for forward Compton scattering. These pioneering works laid the foundation for numerous sum rules for the forward RCS amplitude, obtained by combining DRs with low-energy theorems [29, 30]; see [4, 7] for more detailed discussions. More recently, DRs for non-forward RCS have become a practical tool for extracting information on the nucleon's static polarizabilities from RCS observables from low energies up to the $\Delta(1232)$ resonance region. The formalism has been developed and applied to data using both unsubtracted DRs [31] and subtracted DRs [32, 33]. The unsubtracted DR formalism has also been extended to VCS in [34, 35] and used to extract GPs from VCS data, as recently reviewed in [26].

In the unsubtracted VCS DR formalism of [34, 35], the twelve VCS amplitudes are separated into Born contributions, corresponding to a nucleon intermediate state in the Compton process, and non-Born contributions, corresponding to all intermediate excited states. These non-Born contributions are represented by unsubtracted fixed- t dispersion integrals over their s -channel discontinuities, which are saturated at moderate energies by πN intermediate states. For three of the twelve VCS amplitudes, these s -channel integrals are supplemented at higher energies by energy-independent asymptotic contri-

butions. The asymptotic contributions correspond physically to the t -channel exchange of the π^0 state and the $\pi\pi$ state in the $f_0(500)$ channel, as well as s -channel dispersive contributions beyond the πN state. Although this approach provides a good description of existing VCS data up to the center of mass energy $\simeq 1.25$ GeV, it also highlights a limitation of the unsubtracted formalism: the amplitudes corresponding to the π^0 and $\pi\pi$ t -channel exchanges do not decrease sufficiently fast at high energies for the corresponding integrals to converge. In the unsubtracted DR approaches for RCS [31] and VCS [35], this issue was addressed by evaluating the s -channel dispersion integrals up to a finite cutoff and approximating the remainder by effective t -channel poles. The associated model dependence of this unsubtracted finite-energy sum rule scheme is difficult to quantify reliably, especially for the description of the $\pi\pi$ t -channel exchange through an effective $f_0(500)$ pole exchange, and becomes a limiting factor. To improve on this point, a fixed- t once-subtracted DR formalism was developed for RCS [4, 32]. Due to the extra subtraction in the s -channel dispersive integrals, the corresponding amplitudes then exhibit fast convergence at the expense of introducing two t -dependent subtraction functions. The latter are calculated for zero value of the crossing-symmetric energy (corresponding to the Mandelstam variable condition $s = u$) by once-subtracted DRs in t for the crossed $\gamma\gamma \rightarrow N\bar{N}$ process. In the RCS work of [4, 32], one of these subtraction functions was saturated by the π^0 -pole, while the other was calculated through the $\gamma\gamma \rightarrow \pi\pi \rightarrow N\bar{N}$ process using a dispersive amplitude for the $\gamma\gamma \rightarrow \pi\pi$ process, constrained by data for this reaction and convoluted with the $\pi\pi \rightarrow N\bar{N}$ amplitude taken from [36]. The leading left-hand cut contributions to the subtraction functions were modeled by $\Delta(1232)$ exchange in the s - and u -channels. In the subtracted DR formalism, the subtraction constants at $s = u$ and $t = 0$ can be written directly in terms of the leading scalar and spin polarizabilities, which can then be obtained from a fit to RCS data.

Since the development of the subtracted DR formalism for RCS nearly three decades ago, major progress has been achieved in the dispersive description of the relevant t -channel dynamics. The amplitudes for the real and virtual photon-photon fusion processes $\gamma\gamma \rightarrow \pi\pi$ and $\gamma\gamma^* \rightarrow \pi\pi$ have been analyzed within single- and coupled-channel dispersive frameworks that include $\pi\pi$ rescattering in s - and d -waves and allow for a data-driven description of scalar and tensor isoscalar resonances [37–42]. In parallel, the $\pi\pi \rightarrow N\bar{N}$ partial waves that enter the t -channel discontinuity of the Compton amplitudes have been reconstructed with high precision from the Roy-Steiner equations for πN scattering [43], providing a modern alternative to the older Höhler parameterization [36], extending the range in t up to around 4 GeV². These developments allow us to extend the subtracted DR formalism to the VCS process and suggest that a more constrained and quantitatively controlled disper-

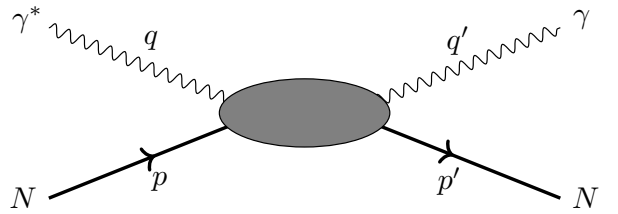


Figure 1: The virtual Compton scattering process on a nucleon.

sive treatment, where the dominant t -channel contributions are anchored to experimental information, is now within reach. The aim of the present work is to mirror the successful subtracted DR approach for RCS [4, 32] and to construct a largely data-driven subtracted DR formalism for VCS from threshold up to the $\Delta(1232)$ -resonance region, in view of the precision goals of present and near-future VCS experiments at Jefferson Lab (JLab) [44, 45].

The paper is organized as follows. In Section II we briefly review the VCS process and the definition of generalized polarizabilities. Section III presents the dispersive formalism for VCS. We first briefly summarize the unsubtracted approach with asymptotic contributions and then develop the once-subtracted fixed- t DRs together with the t -channel DRs for the subtraction functions. In Section IV we provide numerical results for the VCS amplitudes and illustrate their impact on the latest VCS observables from JLab, including comparisons with the unsubtracted framework and studies of sensitivity to the t -channel input. Section V contains our conclusions and outlook. Further technical details of the formalism are given in three Appendices.

II. VIRTUAL COMPTON SCATTERING AND GENERALIZED POLARIZABILITIES

Virtual Compton Scattering (VCS) describes the subprocess

$$\gamma^*(q) + N(p) \rightarrow \gamma(q') + N(p'), \quad (1)$$

where a space-like virtual photon with four-momentum q scatters off a nucleon with mass M_N and four-momentum p , producing a real photon and a nucleon in the final state with four-momenta q' and p' , respectively; see Fig. 1. We denote the initial photon's space-like virtuality by $q^2 = -Q^2 < 0$.

The Mandelstam invariants for the VCS process are given by

$$s = (p + q)^2, \quad t = (q - q')^2, \quad u = (p - q')^2, \quad (2)$$

with the constraint $s + t + u = 2M_N^2 - Q^2$. In describing the VCS process, it is useful to introduce the crossing energy variable ν as

$$\nu = \frac{s - u}{4M_N}. \quad (3)$$

Furthermore, to describe VCS observables, it is common to use the γ^*N center-of-mass (c.m.) frame. In this frame, the c.m. energy W and the angle θ of the outgoing photon momentum direction \hat{q}' relative to the virtual photon momentum direction \hat{q} , can be expressed in terms of Lorentz invariants as

$$W \equiv \sqrt{s}, \quad (4)$$

$$\cos \theta \equiv \hat{q} \cdot \hat{q}' = \frac{1}{\lambda^{1/2}(W^2, M_N^2, -Q^2)} \times \left\{ W^2 - M_N^2 - Q^2 + \frac{2W^2(t + Q^2)}{W^2 - M_N^2} \right\},$$

with the Källén function,

$$\lambda(x, y, z) = x^2 + y^2 + z^2 - 2xy - 2xz - 2yz. \quad (5)$$

Experimentally, the VCS process can be accessed through the $eN \rightarrow e\gamma N$ reaction, as shown in Fig. 2. At leading order $\mathcal{O}(e^3)$ in the electromagnetic coupling, the $eN \rightarrow e\gamma N$ reaction contains both the Bethe-Heitler (BH) subprocess and the VCS subprocess. In the BH subprocess, the real photon is emitted from the lepton line, and the virtual photon has four-momentum $q - q'$, with spacelike virtuality t . It can be calculated exactly in terms of QED and the nucleon elastic form factors [25]. The VCS subprocess is described by the invariant amplitude

$$\mathcal{M}_{\text{VCS}} = \bar{u}(k', h') (-ieq_l \gamma_\mu) u(k, h) \left(\frac{-i}{q^2} \right) \varepsilon_\nu^*(q', \lambda') \times (-ie^2) \bar{N}(p', s') \mathcal{M}^{\mu\nu} N(p, s), \quad (6)$$

where $u(k, h)$ ($\bar{u}(k, h)$) are the initial (final) electron spinors with four-momenta k (k') and helicities h (h') respectively, and $N(p, s)$ ($\bar{N}(p', s')$) are the initial (final) nucleon spinors with four-momenta p (p') and helicities s (s'), respectively; and $\varepsilon_\nu^*(q', \lambda')$ is the final photon polarization vector with four-momentum q' and helicity λ' . Furthermore, in Eq. (6) we introduced a lepton charge factor $q_l = -1$ ($q_l = +1$) for an electron (positron) beam, with $e > 0$ denoting the magnitude of the electric charge unit.

The VCS tensor $\mathcal{M}^{\mu\nu}$ in Eq. (6) can be decomposed into a Born (B) part, corresponding to a nucleon intermediate state, and a non-Born (NB) part, as discussed in [10]. Following the early work of [46], Refs [11, 47] showed how $\mathcal{M}^{\mu\nu}$ can be expressed in a gauge-invariant tensor basis

$$\mathcal{M}^{\mu\nu} = \sum_{i=1}^{12} f_i(Q^2, \nu, t) \rho_i^{\mu\nu}, \quad (7)$$

where the 12 independent gauge-invariant tensors $\rho_i^{\mu\nu}$ are given in Appendix A of [35]. The basis is chosen such that the non-Born parts of the invariant amplitudes $f_i(Q^2, \nu, t)$ are free of kinematic singularities and constraints [11, 47]. The Born terms for the amplitudes are collected in Appendix B of [35].

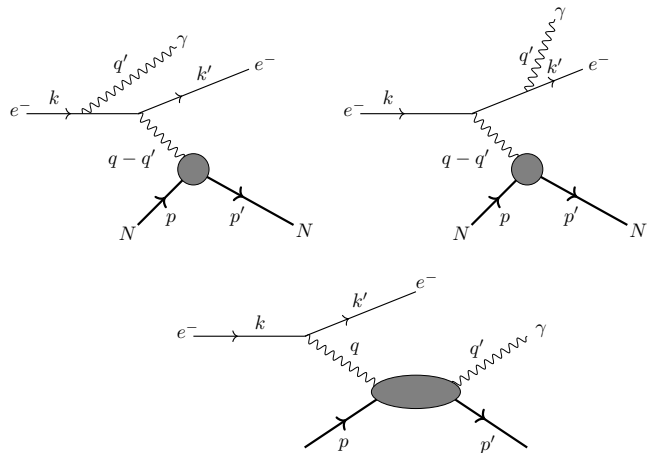


Figure 2: The $eN \rightarrow e\gamma N$ process: Bethe-Heitler process (upper diagrams) and VCS process (lower diagram).

The invariant amplitudes f_i have the following behavior under nucleon crossing combined with charge conjugation ($\nu \rightarrow -\nu$) [35]

$$f_i(Q^2, \nu, t) = f_i(Q^2, -\nu, t), \quad (i = 1, 2, 5, 6, 7, 9, 11, 12),$$

$$f_i(Q^2, \nu, t) = -f_i(Q^2, -\nu, t), \quad (i = 3, 4, 8, 10). \quad (8)$$

Furthermore, in [35] the amplitudes $F_i(Q^2, \nu, t)$ were conveniently introduced, which are all even functions in ν ,

$$F_i(Q^2, \nu, t) \equiv f_i(Q^2, \nu, t), \quad (i = 1, 2, 5, 6, 7, 9, 11, 12),$$

$$F_i(Q^2, \nu, t) \equiv \frac{1}{\nu} f_i(Q^2, \nu, t), \quad (i = 3, 4, 8, 10). \quad (9)$$

Note that, since the odd f_i vanish at $\nu = 0$, the corresponding $F_{i=3,4,8,10}$ are regular there.

For finite initial photon virtuality Q^2 , the limit of a low outgoing photon four-momentum, $q' \rightarrow 0$, corresponds to the kinematic point $\nu = 0, t = -Q^2$. In this limit, the non-Born VCS amplitudes F_i^{NB} can be parameterized in terms of six generalized polarizabilities (GPs) [10, 11]. A convenient choice and multipole notation were proposed in [25]. The relations between these six GPs and the invariant amplitudes are

$$P^{(L1, L1)0}(Q^2) = \sqrt{\frac{2}{3}} N_q \left[\bar{F}_1 + 4M_N^2(1 + \tau)\bar{F}_2 + 4M_N^2\tau(2\bar{F}_6 + \bar{F}_9 - \bar{F}_{12}) \right], \quad (10)$$

$$P^{(M1, M1)0}(Q^2) = -\sqrt{\frac{8}{3}} N_q \bar{F}_1, \quad (11)$$

$$P^{(L1, L1)1}(Q^2) = -\frac{2}{3} N_q M_N \tau \left[\left(\bar{F}_5 + \bar{F}_7 + 4\bar{F}_{11} \right) + 4M_N \bar{F}_{12} \right], \quad (12)$$

$$P^{(M1, M1)1}(Q^2) = -\frac{2}{3} N_q \frac{M_N \tau}{1 + \tau} \left[\bar{F}_5 - 2M_N \tau \bar{F}_{12} \right], \quad (13)$$

$$P^{(M1,L2)1}(Q^2) = \frac{2\sqrt{2}}{3\sqrt{3}}N_q \left[-\frac{1}{2(1+\tau)}\bar{F}_5 + \frac{1}{2}(\bar{F}_5 + \bar{F}_7 + 4\bar{F}_{11}) + \frac{M_N\tau}{1+\tau}\bar{F}_{12} \right], \quad (14)$$

$$P^{(L1,M2)1}(Q^2) = -\frac{\sqrt{2}}{6} \frac{N_q}{1+\tau} \left[4M_N(2\bar{F}_6 + \bar{F}_9) + (\bar{F}_7 + 4\bar{F}_{11}) + 2M_N\tau\bar{F}_{12} \right], \quad (15)$$

where we introduced the shorthand notations

$$\bar{F}_i(Q^2) \equiv F_i^{\text{NB}}(Q^2, \nu=0, t=-Q^2), \quad (16)$$

$$N_q \equiv \left(\frac{1+\tau}{1+2\tau} \right)^{1/2}, \quad \tau \equiv \frac{Q^2}{4M_N^2}.$$

In the GPs $P^{(\rho'L',\rho L)S}$ we used the multipole notation of Refs. [10, 11]: $\rho(\rho')$ denotes the longitudinal (L) or magnetic (M) nature of the initial (final) photon. The initial (final) orbital angular momentum is labeled by $L(L')$, and $S=0,1$ denotes non-spin-flip/spin-flip transition.

It is also convenient to introduce the Q^2 dependent generalizations of the electric dipole (α_{E1}) and magnetic dipole (β_{M1}) polarizabilities as

$$\alpha_{E1}(Q^2) = -\frac{e^2}{4\pi} \sqrt{\frac{3}{2}} P^{(L1,L1)0}(Q^2), \quad (17)$$

$$\beta_{M1}(Q^2) = -\frac{e^2}{4\pi} \sqrt{\frac{3}{8}} P^{(M1,M1)0}(Q^2). \quad (18)$$

In the limit $Q^2 \rightarrow 0$ for the GPs, one finds the following relations with the static polarizabilities as measured in real Compton scattering (RCS)

$$\begin{aligned} \alpha_{E1}(0) &= \alpha_{E1}, \\ \beta_{M1}(0) &= \beta_{M1}, \\ P^{(M1,L2)1}(0) &= -\frac{4\pi}{e^2} \frac{2\sqrt{2}}{3\sqrt{3}} \gamma_{M1E2}, \\ P^{(L1,M2)1}(0) &= -\frac{4\pi}{e^2} \frac{\sqrt{2}}{3} \gamma_{E1M2}, \\ P^{(L1,L1)1}(0) &= 0, \\ P^{(M1,M1)1}(0) &= 0, \end{aligned} \quad (19)$$

where α_{E1} (β_{M1}) are the electric (magnetic) scalar dipole polarizabilities respectively, and where γ_{M1E2} and γ_{E1M2} are two of the four lowest-order spin polarizabilities of the nucleon [4].

III. DISPERSION RELATIONS FOR VCS AMPLITUDES

In [35], a fixed- t dispersive framework was presented for the non-Born VCS amplitudes F_i^{NB} , which are free of kinematical singularities and constraints. To obtain

the corresponding dispersion relations, one needs to start from the analytic structure of the full amplitudes, which includes nucleon pole terms and the s -channel cut contributions starting at the πN threshold (see Fig. 3).

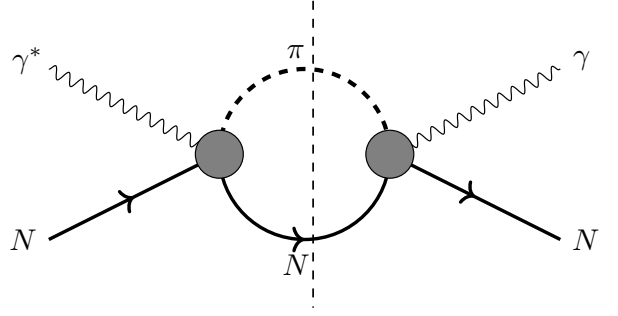


Figure 3: The s -channel πN cut contribution in the dispersive formalism for VCS on the nucleon.

The nucleon poles are located at $s = M_N^2$ and $u = M_N^2$ and are expressed in terms of the crossing variable ν as

$$\begin{aligned} s - M_N^2 &= 2M_N(\nu - \nu_N), \\ u - M_N^2 &= -2M_N(\nu + \nu_N), \end{aligned} \quad (20)$$

with the s -channel nucleon pole position

$$\nu_N = \frac{Q^2 + t}{4M_N}. \quad (21)$$

When evaluating the non-Born VCS amplitudes in the dispersive framework, we need the difference between the pole ($F_i^{s\text{-pole}}$) and Born (F_i^{B}) amplitudes, which are given by

$$\begin{aligned} F_1^{s\text{-pole}}(Q^2, \nu, t) - F_1^{\text{B}}(Q^2, \nu, t) &= -\frac{\kappa F_P(Q^2)}{4M_N^3}, \\ F_5^{s\text{-pole}}(Q^2, \nu, t) - F_5^{\text{B}}(Q^2, \nu, t) &= +\frac{\kappa F_P(Q^2)}{4M_N^4}, \\ F_{11}^{s\text{-pole}}(Q^2, \nu, t) - F_{11}^{\text{B}}(Q^2, \nu, t) &= -\frac{\kappa F_P(Q^2)}{16M_N^4}, \\ F_i^{s\text{-pole}} - F_i^{\text{B}} &= 0, \text{ for } i = 2, 3, 4, 6, 7, 8, 9, 10, 12, \end{aligned} \quad (22)$$

where κ is the nucleon anomalous magnetic moment and $F_P(Q^2)$ is its Pauli form factor, with $F_P(0) = \kappa$. One notices from Eq. (22) that for the combination $F_5 + 4F_{11}$ the difference between pole and Born contribution vanishes, i.e.

$$(F_5 + 4F_{11})^{s\text{-pole}} - (F_5 + 4F_{11})^{\text{B}} = 0. \quad (23)$$

Therefore, we only need to account for the difference between the pole and Born contributions for two combinations out of the twelve VCS amplitudes, which we take as F_1 and F_5 . One furthermore notices from Eq. (22) that the difference between the nucleon pole and Born terms

is energy independent. Consequently, for all twelve VCS amplitudes F_i ($i = 1, \dots, 12$), the following relation holds

$$\begin{aligned} F_i^{s\text{-pole}}(Q^2, \nu, t) - F_i^{\text{B}}(Q^2, \nu, t) \\ = F_i^{s\text{-pole}}(Q^2, 0, t) - F_i^{\text{B}}(Q^2, 0, t). \end{aligned} \quad (24)$$

The s -channel cut contributions in the dispersive formalism start at the πN threshold position ν_0 , given by

$$\nu_0 = \nu_N + m_\pi + \frac{m_\pi^2}{2M_N}, \quad (25)$$

with m_π the pion mass. The convergence of the s -channel dispersion integrals depends on the high-energy behavior of the VCS amplitudes F_i^{NB} . For amplitudes that decrease sufficiently fast at high energy, analyticity allows one to express their real parts, at fixed values of t and Q^2 , through an unsubtracted dispersion integral over the s -channel discontinuity as

$$\begin{aligned} F_i^{\text{NB}}(Q^2, \nu, t) = F_i^{s\text{-pole}}(Q^2, \nu, t) - F_i^{\text{B}}(Q^2, \nu, t) \\ + \frac{2}{\pi} \int_{\nu_0}^{\infty} d\nu' \frac{\nu' \text{Im}_s F_i(Q^2, \nu', t)}{\nu'^2 - \nu^2 - i\varepsilon}, \end{aligned} \quad (26)$$

where ν_0 denotes the pion production threshold.

From the high-energy Regge behavior of the VCS invariant amplitudes ($\nu \rightarrow \infty$ at fixed t and Q^2), it was found in [35] that the amplitudes F_1^{NB} and F_5^{NB} do not drop fast enough in ν for the unsubtracted dispersion integral in Eq. (26) to hold. The leading physical contributions responsible for this behavior are the t -channel $\pi\pi$ exchange with scalar and tensor quantum numbers in F_1^{NB} and the t -channel π^0 pole contribution in F_5^{NB} . In the formalism developed in [35], the unsubtracted dispersion integrals for the VCS amplitudes F_1^{NB} and F_5^{NB} were implemented within a finite-energy sum-rule scheme: the unsubtracted integrals were evaluated up to an upper cutoff, and the remaining high-energy part was approximated by asymptotic contributions, as discussed below. Although this approach describes existing VCS data well from threshold up to the $\Delta(1232)$ region, it introduces a model dependence associated with the treatment of the high-energy contributions. In view of the precision goals of present and forthcoming VCS measurements, and to potentially extend the applicability range of the theory, we instead develop a subtracted dispersion-relation framework for F_1^{NB} and F_5^{NB} , which improves convergence. If the subtraction functions can be constrained by data (or by dispersive input), the resulting framework enables a more transparent propagation of uncertainties.

We will next review the unsubtracted DR formalism with asymptotic contributions as used in [35], and subsequently develop the subtracted DR formalism.

A. Unsubtracted dispersion formalism with asymptotic contributions

Since Ref. [35] aimed to present a VCS DR formalism up to $\Delta(1232)$ resonance energies, the dispersion inte-

grals of Eq. (26) were evaluated only up to a finite upper limit $\nu \leq \nu_{\text{max}}$, with ν_{max} corresponding to the limit $W_{\text{max}} = 2$ GeV. The s -channel discontinuities were saturated by their πN contributions, as shown in Fig. 3. For most VCS amplitudes, this procedure provides a rapidly convergent representation. However, for the amplitudes F_1^{NB} and F_5^{NB} , the unsubtracted dispersion integrals of Eq. (26) do not converge due to their high-energy behavior. In addition, for the amplitude F_2^{NB} , contributions from intermediate states beyond πN are non-negligible and must be accounted for. To handle these cases, Ref. [35] approximated the remaining high-energy part of the s -channel integral ($\nu > \nu_{\text{max}}$) by energy-independent asymptotic contributions.

For the amplitudes F_1^{NB} , the asymptotic contribution was parameterized through an effective t -channel $f_0(500)$ -pole, with a Q^2 -dependent residue adjusted to reproduce the Q^2 dependence of the GP $\beta_{M1}(Q^2)$.

For the amplitude F_5^{NB} , the asymptotic contribution was parameterized through the t -channel π^0 -pole contribution in terms of the $\gamma^*\gamma \rightarrow \pi^0$ transition form factor.

For the amplitudes F_2^{NB} , the asymptotic contribution was adjusted to reproduce the Q^2 dependence of the GP combination $\alpha_{E1}(Q^2) + \beta_{M1}(Q^2)$.

B. Subtracted dispersion relation formalism

To overcome the convergence limitations of the unsubtracted framework [35], we now develop a once-subtracted fixed- t DR formalism. For the non-Born VCS amplitudes F_1^{NB} , F_5^{NB} , and for a specific combination involving F_2^{NB} as defined below, the unsubtracted DR of Eq. (26) is either not valid or converges too slowly. We therefore write a once-subtracted fixed- t dispersion relation

$$\begin{aligned} F_i^{\text{NB}}(Q^2, \nu, t) = F_i^{\text{NB}}(Q^2, 0, t) \\ + \frac{2}{\pi} \nu^2 \int_{\nu_0}^{\infty} d\nu' \frac{\text{Im}_s F_i(Q^2, \nu', t)}{\nu'(\nu'^2 - \nu^2 - i\varepsilon)}, \end{aligned} \quad (27)$$

where the subtraction is performed at $\nu = 0$. Owing to Eq. (24), the difference between pole and Born contributions cancels in this relation.

The subtraction function $F_i^{\text{NB}}(Q^2, 0, t)$ in Eq. (27) is then evaluated through a once-subtracted DR in the variable t at fixed Q^2 . Choosing the subtraction point at $t = -Q^2$, we obtain the following subtracted DRs in the variable t :

$$\begin{aligned} F_i^{\text{NB}}(Q^2, 0, t) = F_i^{\text{NB}}(Q^2, 0, -Q^2) \\ + F_i^{t\text{-pole}}(Q^2, 0, t) - F_i^{t\text{-pole}}(Q^2, 0, -Q^2) \\ + \frac{(t + Q^2)}{\pi} \int_{t_R}^{\infty} dt' \frac{\text{Im}_t F_i(Q^2, 0, t')}{(t' + Q^2)(t' - t - i\varepsilon)} \\ + \frac{(t + Q^2)}{\pi} \int_{-\infty}^{t_L} dt' \frac{\text{Im}_t F_i(Q^2, 0, t')}{(t' + Q^2)(t' - t - i\varepsilon)}. \end{aligned} \quad (28)$$

We will subsequently discuss the four contributions on the right-hand side (*rhs*) of Eq. (28).

The first contribution on the *rhs* of Eq. (28) is the non-Born VCS amplitudes evaluated at the subtraction point $t = -Q^2$. Using Eqs. (10) - (15), these can be expressed in terms of GPs for the following six combinations of VCS amplitudes

$$\begin{aligned} & F_1^{\text{NB}}, \quad F_2^{\text{NB}}, \quad F_5^{\text{NB}}, \quad F_5^{\text{NB}} + F_7^{\text{NB}} + 4F_{11}^{\text{NB}}, \\ & 2F_6^{\text{NB}} + F_9^{\text{NB}}, \quad F_{12}^{\text{NB}}. \end{aligned} \quad (29)$$

In this work, we will evaluate the subtracted DRs of Eqs. (27) and (28) for the amplitudes F_1^{NB} , F_5^{NB} , and for the combination

$$\tilde{F}_2^{\text{NB}} \equiv F_2^{\text{NB}} - \frac{t}{4M_N^2 - t} \left(2F_6^{\text{NB}} + F_9^{\text{NB}} - F_{12}^{\text{NB}} \right). \quad (30)$$

For these three amplitudes, their values at the subtraction point can be expressed in terms of GPs as

$$F_1^{\text{NB}}(Q^2, 0, -Q^2) = \frac{4\pi}{e^2} \frac{1}{N_q} \beta_{M1}(Q^2), \quad (31)$$

$$\begin{aligned} \tilde{F}_2^{\text{NB}}(Q^2, 0, -Q^2) &= -\frac{4\pi}{e^2} \frac{1}{N_q} \frac{1}{4M_N^2(1+\tau)} \\ &\times \left\{ \alpha_{E1}(Q^2) + \beta_{M1}(Q^2) \right\}, \end{aligned} \quad (32)$$

$$\begin{aligned} F_5^{\text{NB}}(Q^2, 0, -Q^2) &= -\frac{1}{N_q} \frac{3}{4M_N} \left\{ P^{(L1, L1)1}(Q^2) \right. \\ &+ \left(\frac{2+\tau}{\tau} \right) P^{(M1, M1)1}(Q^2) \\ &\left. + 2M_N \tau \sqrt{\frac{3}{2}} P^{(M1, L2)1}(Q^2) \right\}. \end{aligned} \quad (33)$$

The second contribution on the *rhs* of Eq. (28) is due to the π^0 t -channel pole and is non-zero only for the amplitudes F_5^{NB} and F_{11}^{NB}

$$\begin{aligned} F_5^{t\text{-pole}}(Q^2, 0, t) &= -4F_{11}^{t\text{-pole}}(Q^2, 0, t), \\ &= \frac{g_{\pi NN}}{M_N} \frac{1}{t - m_\pi^2} F_{\pi^0 \gamma^* \gamma}(Q^2), \end{aligned} \quad (34)$$

with πNN coupling given by $g_{\pi NN} = 13.13$, and where $F_{\pi^0 \gamma^* \gamma}(Q^2)$ is the $\gamma^* \gamma \rightarrow \pi^0$ transition form factor parameterized through the monopole form

$$F_{\pi^0 \gamma^* \gamma}(Q^2) = F_{\pi^0 \gamma^* \gamma}(0) \frac{1}{1 + Q^2/\Lambda_\pi^2}. \quad (35)$$

We use the fit to the space-like single virtual $\gamma^* \gamma \rightarrow \pi^0$ world data up to $Q^2 < 9 \text{ GeV}^2$ with values [48]

$$\begin{aligned} \Lambda_\pi^2 &= (0.611 \pm 0.005) \text{ GeV}^2, \\ F_{\pi^0 \gamma^* \gamma}(0) &= (0.273 \pm 0.003) \text{ GeV}^{-1}. \end{aligned} \quad (36)$$

Note that Eq. (34) implies that the π^0 pole contribution drops out of the combination $F_5^{\text{NB}} + 4F_{11}^{\text{NB}}$. Furthermore,

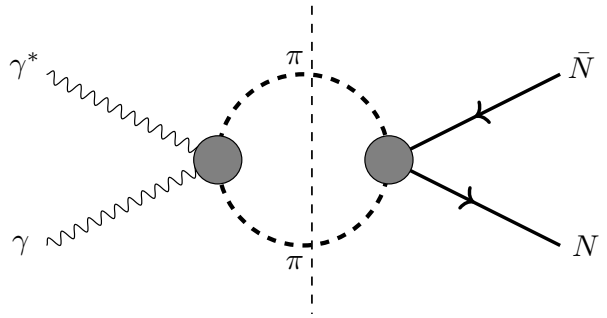


Figure 4: The t -channel $\pi\pi$ right-hand cut contribution in the subtracted dispersive formalism for VCS on the nucleon.

for the amplitude F_5 , the difference $F_5^{\text{NB}}(Q^2, 0, -Q^2) - F_5^{t\text{-pole}}(Q^2, 0, -Q^2)$ entering Eq. (28) can be expressed, using Eq. (33), in terms of the dispersive spin GP contribution, i.e. beyond the π^0 pole.

The third and fourth contributions on the *rhs* of Eq. (28) arise from the discontinuities across the t -channel right-hand cut and left-hand cut, respectively. The right-hand cut starts at the $\pi\pi$ threshold, $t_R = 4m_\pi^2$, and extends along the positive real t -axis. The left-hand cut extends along the negative real t -axis and starts at

$$t_L = -2m_\pi^2 - 4M_N m_\pi - Q^2, \quad (37)$$

which corresponds to the πN threshold for $\nu = 0$. For $t < t_L$, the left-hand-cut term in Eq. (28) has to be understood with the $t \rightarrow t + i\epsilon$ prescription. It then decomposes into a principal-value integral giving the real part, and an additional imaginary part $i \text{Im}_t F_i(Q^2, 0, t)$ on the cut. The principal-value part can be evaluated numerically as

$$\begin{aligned} & \frac{(t+Q^2)}{\pi} \mathcal{P} \int_{-\infty}^{t_L} dt' \frac{\text{Im}_t F_i(Q^2, 0, t')}{(t'+Q^2)(t'-t)} \\ &= \frac{(t+Q^2)}{\pi} \int_{-\infty}^{t_L} dt' \frac{\text{Im}_t F_i(Q^2, 0, t') - \text{Im}_t F_i(Q^2, 0, t)}{(t'+Q^2)(t'-t)} \\ &+ \frac{1}{\pi} \text{Im}_t F_i(Q^2, 0, t) \ln \left| \frac{t_L - t}{t_L + Q^2} \right|. \end{aligned} \quad (38)$$

In the next two subsections, we will discuss in detail how to estimate the t -channel right- and left-hand cuts.

C. t -channel right-hand cut contribution due to $\pi\pi$ intermediate state

The leading t -channel right-hand cut contribution to the VCS amplitudes at $\nu = 0$ arises from the $\pi\pi$ intermediate state (see Fig. 4). In Appendix B, we express the corresponding discontinuities of the VCS amplitudes in terms of the helicity amplitudes for the processes $\gamma^* \gamma \rightarrow \pi\pi$ and $\pi\pi \rightarrow N\bar{N}$.

For the $\gamma^* \gamma \rightarrow \pi\pi$ amplitudes, we use the s - and d -wave amplitudes of the dispersive formalism of [40],

which provides a good description of the available $\gamma\gamma \rightarrow \pi\pi$ data from threshold up to $\pi\pi$ invariant mass of 1.4 GeV, and which was extended to the processes with one or both photons having spacelike virtuality [42].

For the $\pi\pi \rightarrow N\bar{N}$ amplitudes, two sets of s and d -wave amplitudes are available. The older reconstruction of Höhler [36] is given up to $t \lesssim 0.78 \text{ GeV}^2$ and was used in the RCS subtracted DR formalism of [32]. In the more recent analysis of Hoferichter *et al.* [43], which we employ here, the s - and d -wave amplitudes were reconstructed from Roy-Steiner equations for πN scattering and provided up to $t \lesssim 4 \text{ GeV}^2$.

Both the dispersive framework for $\gamma^*\gamma \rightarrow \pi\pi$ and the modern Roy-Steiner reconstruction for $\pi\pi \rightarrow N\bar{N}$ incorporate a coupled-channel description in the scalar-isoscalar channel ($I = 0$, s -wave), and therefore cover both the $f_0(500)$ and $f_0(980)$ regions. In the present work, however, we restrict ourselves to the dominantly elastic $\pi\pi$ contribution in the s -wave. Therefore, when evaluating the t -channel right-hand cut integrals of Eq. (28) for the s -wave, we truncate the dispersive integration at 0.78 GeV^2 , i.e., we keep only the elastic $f_0(500)$ region, below the onset of significant inelasticities. For the d -wave, both the $\gamma^*\gamma \rightarrow \pi\pi$ and $\pi\pi \rightarrow N\bar{N}$ inputs are based on single-channel analyses covering the $f_2(1270)$ region and are reliable up to at least 2 GeV^2 . Although the $\gamma^*\gamma \rightarrow \pi\pi$ and $\pi\pi \rightarrow N\bar{N}$ inputs are obtained from independent dispersive analyses, both rely on $\pi\pi$ phase-shift information constrained by Roy-type analyses [49, 50]. As a consequence, Watson's theorem holds in the elastic region, ensuring that the phases cancel in the unitarity relation below. Any residual mismatch in the phase input provides an additional source of systematic uncertainty in the numerical evaluation.

For the three VCS amplitudes F_1^{NB} , \tilde{F}_2^{NB} , and F_5^{NB} , which we evaluate in this work through the subtracted DR formalism, the $\pi\pi$ right-hand cut discontinuities (including s - and d -waves) are obtained from Eq. (B11) as

$$\begin{aligned} \text{Im}_t F_1^{\pi\pi}(Q^2, 0, t') &= -\frac{1}{e^2} \frac{\beta_\pi(t')}{t' + Q^2} \\ &\times \left\{ \frac{1}{4M_N^2 - t'} h_0^0(t', Q^2) f_+^{0*}(t') \right. \\ &\left. + \frac{5}{32} t' \beta_\pi^2(t') \left[h_0^2(t', Q^2) - \sqrt{\frac{3}{2}} h_2^2(t', Q^2) \right] f_+^{2*}(t') \right\}, \end{aligned} \quad (39)$$

$$\begin{aligned} \text{Im}_t \tilde{F}_2^{\pi\pi}(Q^2, 0, t') &= -\frac{1}{e^2} \frac{5}{16} \frac{\beta_\pi^3(t')}{4M_N^2 - t'} \\ &\times \left\{ \sqrt{\frac{3}{2}} \left(\frac{t'}{t' + Q^2} \right) h_2^2(t', Q^2) f_+^{2*}(t') \right. \\ &- \frac{1}{2M_N} \left(\frac{t'}{t' + Q^2} \right)^2 \left[\sqrt{\frac{3}{2}} t' h_0^2(t', Q^2) \right. \\ &\left. \left. + \sqrt{2t'Q^2} h_1^2(t', Q^2) - \frac{Q^2}{2} h_2^2(t', Q^2) \right] f_-^{2*}(t') \right\}, \end{aligned} \quad (40)$$

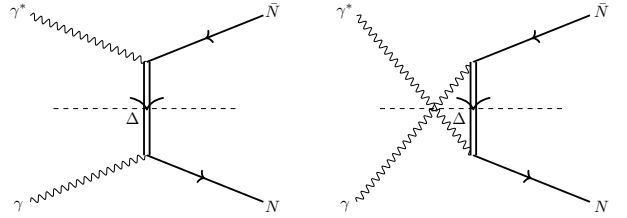


Figure 5: The t -channel $\Delta(1232)$ -resonance exchange left-hand cut contribution in the subtracted dispersive formalism for VCS on the nucleon.

$$\begin{aligned} \text{Im}_t F_5^{\pi\pi}(Q^2, 0, t') &= -\frac{1}{e^2} \left(\frac{t'}{t' + Q^2} \right) \frac{5}{32} \beta_\pi^3(t') \\ &\times \left\{ \left[h_2^2(t', Q^2) - \sqrt{\frac{2t'}{Q^2}} h_1^2(t', Q^2) \right] f_-^{2*}(t') \right\}, \end{aligned} \quad (41)$$

where we defined the pion velocity in the $\pi\pi$ rest frame as

$$\beta_\pi(t') = \sqrt{1 - \frac{4m_\pi^2}{t'}}. \quad (42)$$

In Eqs. (39)-(41), $h_{\Lambda_\gamma}^J(t', Q^2)$ are the isospin $I = 0$ helicity amplitudes for the $\gamma^*\gamma \rightarrow \pi\pi$ process from Ref. [40], where J refers to the partial wave in the $\pi\pi$ system, and Λ_γ is the difference of photon helicities in the $\gamma^*\gamma$ c.m. system. Note that the s -wave $\pi\pi$ intermediate state only contributes to $\text{Im}_t F_1$, whereas $\text{Im}_t \tilde{F}_2$ and $\text{Im}_t F_5$ only receive contributions from d -waves or higher partial waves. Furthermore, $f_\pm^J(t')$ denote the isospin $I = 0$ $\pi\pi \rightarrow N\bar{N}$ helicity amplitudes for parallel (+) or anti-parallel (-) nucleon and anti-nucleon helicities [51].

D. t -channel left-hand cut contribution due to $\Delta(1232)$ -exchange

The leading t -channel left-hand cut contribution to the VCS amplitudes at $\nu = 0$ arises from the πN intermediate state. In this work, we approximate the corresponding left-hand cut discontinuity by the spectral function associated with $\Delta(1232)$ excitation in the s - and u -channels (see Fig. 5) including its finite width, $\Gamma_\Delta = 0.117 \text{ GeV}$. Furthermore, we consider the dominant magnetic dipole excitations in the $\gamma^* N \Delta$ and $\gamma N \Delta$ vertices. Details of the derivation are given in Appendix C.

For the three VCS amplitudes F_1^{NB} , \tilde{F}_2^{NB} , and F_5^{NB} , which we evaluate in this work through a subtracted DR, the left-hand cut discontinuities due to the $\Delta(1232)$ -exchange are obtained from Eqs.(C12)-(C19) as

$$\begin{aligned} \text{Im}_t F_1^\Delta(Q^2, 0, t') &= \left[\pi \rho^\Delta \left(M_N^2 - \frac{1}{2}(t' + Q^2); M_\Delta, \Gamma_\Delta \right) \right] \\ &\times \frac{G_M^*(0) G_M^*(Q^2)}{M_N^2 Q_+^2} \left\{ -2M_N^2 (M_N + M_\Delta) (1 + \tau) \right. \end{aligned}$$

$$+ \left(M_\Delta + \frac{3}{4} M_N \right) (t' + Q^2) \Big\}, \quad (43)$$

$$\begin{aligned} \text{Im}_t \tilde{F}_2^\Delta(Q^2, 0, t') &= \left[\pi \rho^\Delta \left(M_N^2 - \frac{1}{2}(t' + Q^2); M_\Delta, \Gamma_\Delta \right) \right] \\ &\times \frac{G_M^*(0) G_M^*(Q^2)}{M_N^2 Q_+^2} \left\{ \frac{1}{2} (M_N + M_\Delta) \right. \\ &\quad \left. + \frac{M_N}{4(4M_N^2 - t')} (t' + Q^2) \right\}, \quad (44) \end{aligned}$$

$$\begin{aligned} \text{Im}_t F_5^\Delta(Q^2, 0, t') &= \left[\pi \rho^\Delta \left(M_N^2 - \frac{1}{2}(t' + Q^2); M_\Delta, \Gamma_\Delta \right) \right] \\ &\times \frac{G_M^*(0) G_M^*(Q^2)}{M_N^2 Q_+^2} \left\{ -M_N (M_N + M_\Delta) \left(1 + \frac{\tau}{2} \right) \right. \\ &\quad \left. + (M_\Delta + 7M_N) \frac{(t' + Q^2)}{8M_N} \right\}. \quad (45) \end{aligned}$$

where the normalized $\Delta(1232)$ spectral function ρ^Δ is defined in Eq. (C26). The variable Q_+^2 is defined in Eq. (C5), and $G_M^*(Q^2)$ denotes the magnetic dipole transition form factor, for which we use the MAID2007 parameterization given in Eq. (C8).

Because the dispersion relation in t is once-subtracted, the left-hand cut integrals exhibit rapid convergence. For VCS observables up to the $\Delta(1232)$ energy region, as considered in this work, contributions from higher-mass baryon resonances beyond the $\Delta(1232)$ are therefore expected to be suppressed.

IV. RESULTS AND DISCUSSION

We start our discussion with the t -channel dispersive input and the calculation of the subtraction functions at $\nu = 0$ for the non-Born VCS amplitudes F_1^{NB} , \tilde{F}_2^{NB} , and F_5^{NB} , which are the main new elements of the present subtracted DR formalism for VCS. For illustration, the t -dependence of $F_1^{\text{NB}}(Q^2, 0, t)$, $\tilde{F}_2^{\text{NB}}(Q^2, 0, t)$, and $F_5^{\text{NB}}(Q^2, 0, t)$ is shown in Figs. 6, 7, and 8 for $Q^2 = 0.33 \text{ GeV}^2$. Several VCS experiments have taken data at this Q^2 value, including the most recent measurement of Ref. [24].

In the right panels of Figs. 6-8, we show the t -channel discontinuities $\text{Im}_t F_i$ arising from the right-hand cut (RHC) due to the $\pi\pi$ intermediate state (see Sec. III C) and from the left-hand cut (LHC) due to the $\Delta(1232)$ resonance (see Sec. III D). The dominant feature of the RHC input is the s -wave $\pi\pi$ contribution corresponding to the $f_0(500)$ region, which contributes exclusively to $\text{Im}_t F_1$ according to Eq. (39) (see the right panel of Fig. 6). Furthermore, the d -wave $\pi\pi$ state contributes to all three discontinuities and shows a pronounced enhancement due to the tensor resonance $f_2(1270)$. As seen in Fig. 6, the $f_0(500)$ and $f_2(1270)$ contributions to $\text{Im}_t F_1$

enter with opposite sign, leading to a partial cancellation in the evaluating $\text{Re}F_1$.

In this work, the numerical evaluation of both s - and d -wave $\pi\pi$ contributions to the t -channel RHC discontinuities in Eqs. (39)-(41) is performed using the $\gamma^*\gamma \rightarrow \pi\pi$ amplitudes of the dispersive formalism of [40] and the $\pi\pi \rightarrow N\bar{N}$ amplitudes of [43], constructed from the Roy-Steiner equations for πN scattering. In evaluating the corresponding real parts $\text{Re}F_i$, the RHC subtracted dispersion integrals in Eq. (28) are computed up to an upper cutoff $\simeq 2 \text{ GeV}^2$ in d -wave and $\simeq 0.78 \text{ GeV}^2$ in s -wave¹. It was checked that the subtracted dispersion integrals exhibit very fast convergence, and any contribution to $\text{Im}_t F_i$ originating from the timelike region beyond $t \sim 2 \text{ GeV}^2$ has a negligible impact when evaluating $\text{Re}F_i(Q^2, 0, t)$ in the spacelike region for $-t \lesssim 1 \text{ GeV}^2$.

Figures 6-8 also show the LHC discontinuities from the $\Delta(1232)$ resonance and the corresponding LHC subtracted dispersion integrals in Eq. (28). We checked that in evaluating the LHC contribution to $\text{Re}F_i(Q^2, 0, t)$ in the spacelike region for $-t \lesssim 0.8 \text{ GeV}^2$, the corresponding LHC subtracted dispersion integrals exhibit very fast convergence. They reach around 95% or higher of their asymptotic value for the lower integration limit of $t_{\text{lower}} = -3 \text{ GeV}^2$, which corresponds to $W \simeq 1.5 \text{ GeV}$ for $\nu = 0$ and $Q^2 = 0.33 \text{ GeV}^2$. Thus, further LHC discontinuities beyond $\Delta(1232)$ are expected to contribute at the few percent level or less to the subtracted dispersion integral for $\text{Re}F_i(Q^2, 0, t)$.

The good convergence of the subtracted integrals entering $\text{Re}F_i(Q^2, 0, t)$ in Eq. (28) in our subtracted DR formalism is achieved at the expense of introducing the subtraction constants $F_i^{\text{NB}}(Q^2, 0, -Q^2) - F_i^{t\text{-pole}}(Q^2, 0, -Q^2)$. For the amplitude F_1 , the subtraction constant is related to the magnetic GP $\beta_{M1}(Q^2)$ according to Eq. (31), while for the amplitude \tilde{F}_2 it is related to the GP combination $\alpha_{E1}(Q^2) + \beta_{M1}(Q^2)$ according to Eq. (32). In our formalism, both constants are to be extracted from a fit to the VCS data. In Figs. 6 and 7, we illustrate their contribution $\text{Re}F_1$ and $\text{Re}\tilde{F}_2$ using the GP values determined in the JLab experiment of [24]. For the amplitude F_5 , which contains the π^0 pole contribution, the subtraction constant involves the GP contribution beyond the π^0 pole. Its value is expressed in terms of a spin GP according to Eq. (33) and is calculated in the present work using Eq. (26) for $t = -Q^2$ and

¹ In the present implementation we truncate the s -wave $\pi\pi$ contribution at $\simeq 0.78 \text{ GeV}^2$ in order to isolate the $f_0(500)$ region. Extending the s -wave integration to higher cutoff would include the $f_0(980)$ region, where the $\gamma^*\gamma \rightarrow K\bar{K}$ and $K\bar{K} \rightarrow N\bar{N}$ inputs are needed in addition to the $\pi\pi$ channel. We have checked that the $\pi\pi$ contribution remains dominant above the $K\bar{K}$ threshold and omitting $K\bar{K}$ channel induces an imaginary part at the $\sim 15 - 20\%$ level in $\text{Im}_t F_1$. Within our once-subtracted DR framework, the resulting impact of the $f_0(980)$ region on $\text{Re}F_1$ is further suppressed.

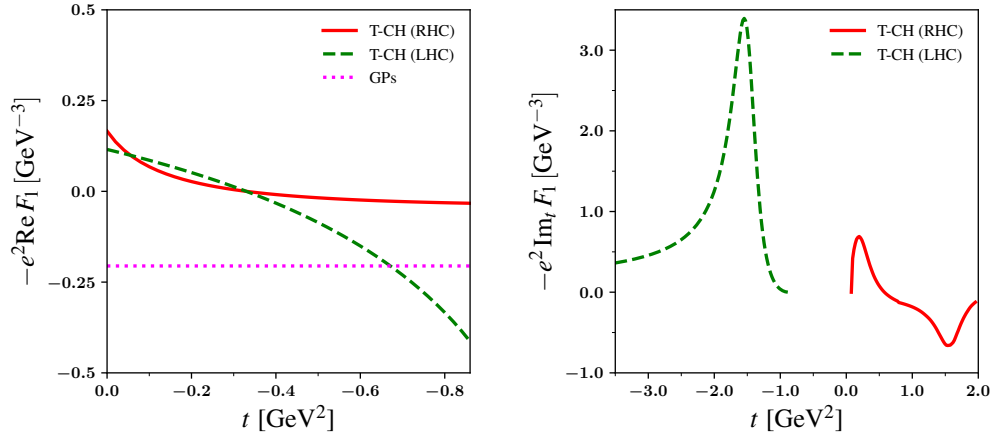


Figure 6: t -channel contributions to the real and imaginary parts of the amplitude $F_1^{\text{NB}}(Q^2, 0, t)$ at $Q^2 = 0.33 \text{ GeV}^2$ as function of t . Left panel: results from the t -channel subtracted DRs according to Eq. (28), with the separate contributions from the right-hand cut (RHC), left-hand cut (LHC), and the subtraction constant. The subtraction constant corresponds with a value of the GP $\beta_{M1}(Q^2) = 1.20 \times 10^{-4} \text{ fm}^3$. Right panel: contributions to the imaginary part from the left-hand and right-hand cuts in the t -channel.

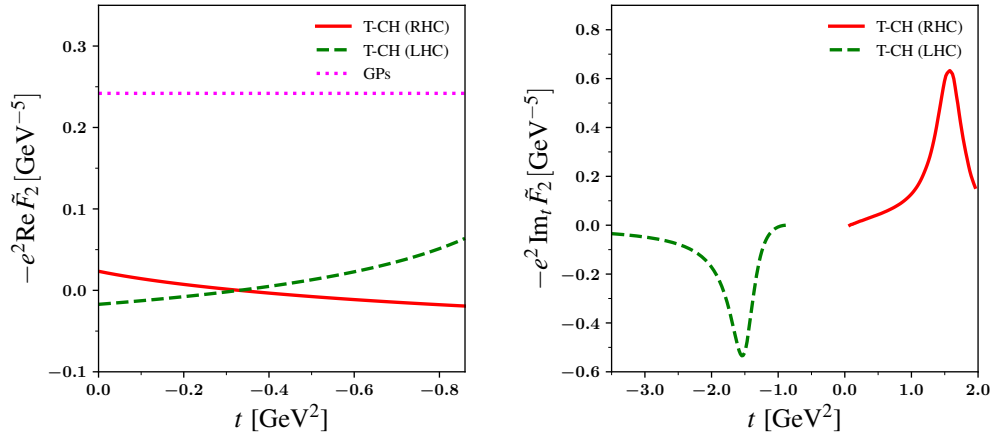


Figure 7: The same as in Fig. 6 but for the amplitude $\tilde{F}_2^{\text{NB}}(Q^2, 0, t)$ at $Q^2 = 0.33 \text{ GeV}^2$. The subtraction constant corresponds with a value of the GP combination $\alpha_{E1}(Q^2) + \beta_{M1}(Q^2) = 5.44 \times 10^{-4} \text{ fm}^3$.

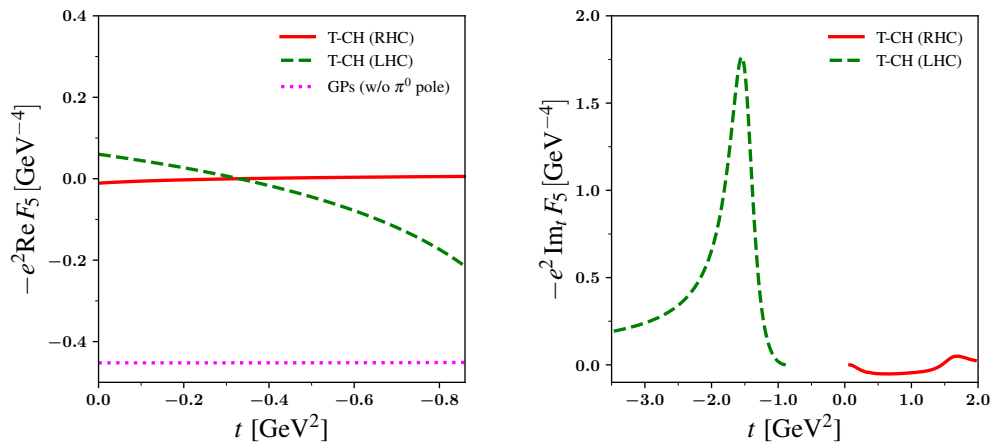


Figure 8: The same as in Fig. 6 but for the amplitude $F_5^{\text{NB}}(Q^2, 0, t)$. The GP value excludes the π^0 pole contribution and is calculated according to Eq. (26) for $t = -Q^2$ and $\nu = 0$, with the upper limit of integration corresponding to $W_{\text{max}} = 2.0 \text{ GeV}$.

$\nu = 0$, with the upper integration limit corresponding to $W_{\max} = 2.0$ GeV.

Extracting the GPs from VCS measurements in the $\Delta(1232)$ energy region requires a reliable control of the W dependence, which is provided by the dispersive calculation. The s -channel dispersive input which enters the subtracted DRs of Eq. (27), as well as the corresponding real parts $\text{Re}F_i$, are shown in Figs. 9, 10, and 11 as functions of the c.m. energy W for $Q^2 = 0.33$ GeV² and for a fixed c.m. scattering angle $\theta = 150^\circ$. Along such a curve of fixed scattering angle, W increases starting at $W = M$, where the amplitudes reduce to their GP values $F_i^{\text{NB}}(Q^2, 0, -Q^2)$. The right panels of Figs. 9, 10, and 11 show the s -channel discontinuities $\text{Im}_s F_i$ entering the subtracted dispersion integrals. One sees that these s -channel discontinuities are dominated by the low- W region where the MAID2007 parameterization [52] provides a very good description of existing pion electroproduction data. For $\text{Im}_s F_1$ and $\text{Im}_s \tilde{F}_2$ the contributions beyond the $\Delta(1232)$ region are very small, while for $\text{Im}_s F_5$ the contributions in the second and third nucleon resonance regions come with opposite sign. Thus, the corresponding subtracted dispersive integral for $\text{Re}F_5$ is also nearly completely saturated by its contribution from the $\Delta(1232)$ region. One sees from the left panels of Figs. 9 and 10 that the real parts of the VCS amplitudes F_1 and \tilde{F}_2 show the characteristic variation of an elastic resonance, with the real part of the s -channel dispersive contribution going through zero when crossing the $\Delta(1232)$ position. The real part of the amplitude F_5 , shown in Fig. 11, displays in addition a pronounced cusp behavior at the πN threshold. On the other hand, the t -channel subtracted DR contribution displays a smooth variation with W for the VCS amplitudes, while $\text{Re}F_5$ shows a prominent π^0 pole contribution. Furthermore, we also show the GP subtraction constant contribution, corresponding to $\text{Re}F_i$ at $W = M$. In the middle panels of Figs. 9, 10, and 11, we compare the present subtracted DR formalism with the unsubtracted DR result of [35]. While there is a good overall agreement between both frameworks in the $\Delta(1232)$ energy region, one notices that in particular on the higher energy side of the $\Delta(1232)$, where the experiment of [24] has taken data, there are clear differences that are significant when compared with the GP effects.

The above mentioned recent JLab VCS experiment of [24] was performed at several fixed W values in the $\Delta(1232)$ region. As illustration, we show in Figs. 12, 13, and 14 for a fixed $W = 1.19$ GeV, fixed $Q^2 = 0.33$ GeV² kinematics of [24] the t -dependence of the VCS amplitudes F_1 , \tilde{F}_2 , and F_5 in the present subtracted DR formalism in comparison with their unsubtracted counterparts from [35]. One again notices clear differences between both formalisms. While for $\text{Re}\tilde{F}_2$ and $\text{Re}F_5$ the differences between the subtracted and unsubtracted results are mainly increasing for larger values of $-t$, for the amplitude $\text{Re}F_1$ there is a clear difference over the whole t -region. This difference mainly originates from the different treatment of the t -channel discontinuities. In the

unsubtracted formalism of [35] the t -channel asymptotic contribution to the amplitude F_1 was modeled through a $f_0(500)$ -pole contribution, leading to a monopole behavior in t . The latter is responsible for the steeper behavior especially at smaller values of $-t$, as seen from the middle panel in Fig. 12. In the present subtracted DR formalism on the other hand, the t -dependence is fully calculated and for $\text{Re}F_1$ is given by the RHC and LHC contributions as shown in Fig. 6 and discussed above. Such different t -dependence is of relevance when extracting the GPs from the VCS data in the $\Delta(1232)$ region.

We next discuss the VCS observables and present our results in the subtracted DR formalism. The unpolarized fivefold differential cross section for the $e^-p \rightarrow e^- \gamma p$ reaction is expressed as [10]

$$\frac{d^5\sigma}{(d\Omega'_e)_L d|\vec{k}'|_L (d\Omega'_p)_{\text{c.m.}}} = \frac{\Phi}{4} \sum_{h,h',s,s',\lambda'} |\mathcal{M}_{\text{BH}} + \mathcal{M}_{\text{VCS}}|^2, \quad (46)$$

where the scattered lepton solid angle ($d\Omega'_e$) and momentum value ($|\vec{k}'|$) are expressed in the Lab (L) frame, in which the proton target is at rest ($\vec{p} = 0$), and where the scattered proton solid angle ($d\Omega'_p$) is expressed in the γ^*p c.m. frame. The phase space factor Φ in Eq. (46) is given by [10]

$$\Phi = \frac{1}{(2\pi)^5} \frac{1}{64M_N} \frac{s - M_N^2}{s} \frac{E'_e}{E_e}, \quad (47)$$

with E_e (E'_e) the beam (scattered) electron energy in the Lab frame. Furthermore, the unpolarized cross section of Eq. (46) involves a helicity average over the squared invariant amplitude of the $e^-p \rightarrow e^- \gamma p$ reaction. The $e^-p \rightarrow e^- \gamma p$ invariant amplitude consists, at order $\mathcal{O}(e^3)$, of two terms: \mathcal{M}_{VCS} describing the VCS subprocess (lower diagram in Fig. 2), given by Eq. (6), and \mathcal{M}_{BH} describing the BH subprocess (top diagrams in Fig. 2). The latter is given by

$$\begin{aligned} \mathcal{M}_{\text{BH}} = & \frac{ie^3}{t} \bar{u}(k', h') \left\{ \gamma^\mu \frac{\gamma \cdot (k - q') + m}{-2k \cdot q'} \gamma^\nu \right. \\ & \left. + \gamma^\nu \frac{\gamma \cdot (k' + q') + m}{2k' \cdot q'} \gamma^\mu \right\} u(k, h) \varepsilon_\nu^*(q', \lambda') \\ & \times \bar{N}(p', s') \left\{ F_D(t) \gamma_\mu + F_P(t) \frac{i\sigma_{\mu\alpha}(q - q')^\alpha}{2M_N} \right\} N(p, s), \end{aligned} \quad (48)$$

with m the lepton mass. On the proton side, the BH amplitude is expressed in terms of the Dirac (F_D) and Pauli (F_P) proton form factors with spacelike argument t , for which we use the parameterization from [53].

The pioneering work of [10] proposed to study the $e^-p \rightarrow e^- \gamma p$ reaction at low c.m. energy W as a tool to extract the nucleon GPs. Specifically, it proposed to make a low-energy expansion (LEX) of the $e^-p \rightarrow e^- \gamma p$

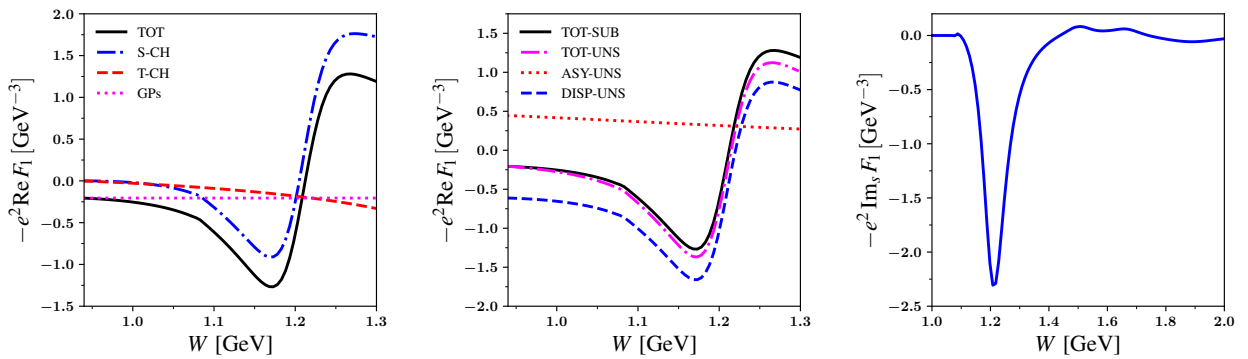


Figure 9: Real and imaginary parts of the amplitude $F_1^{\text{NB}}(Q^2, \nu, t)$ at $Q^2 = 0.33 \text{ GeV}^2$ and $\theta = 150^\circ$ as function of W . Left panel: results from the subtracted DRs with the separate contributions from the s - and t -channel, and for a value of the GP $\beta_{M1}(Q^2) = 1.20 \times 10^{-4} \text{ fm}^3$. Middle panel: total results from subtracted DRs (solid black curve) compared with the unsubtracted DR result of [35] (dashed-dotted pink curve). For the unsubtracted DR result we also show the separate contributions of the dispersive s -channel contribution according to Eq. (26) with the upper limit of integration corresponding to $W_{\text{max}} = 2.0 \text{ GeV}$ (dashed blue curve) and the asymptotic t -channel contribution (dotted red curve). Right panel: contribution to the imaginary part from the s -channel cut.

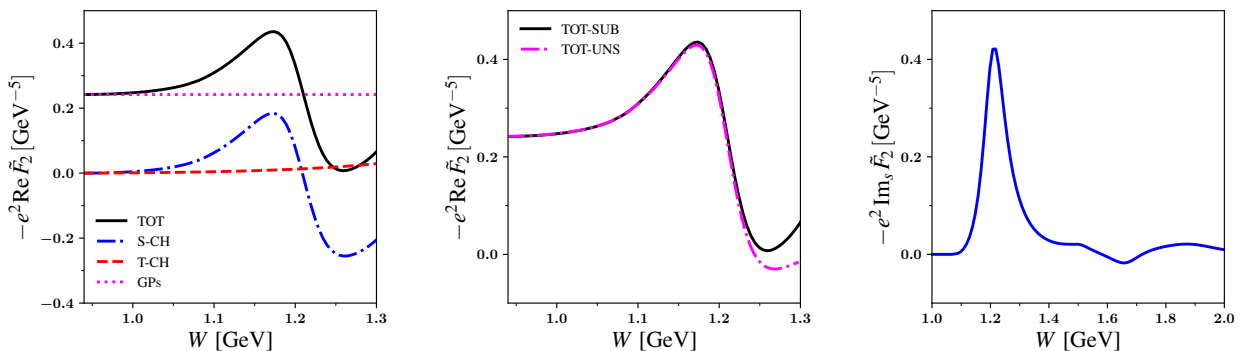


Figure 10: Real and imaginary parts of the amplitude $\tilde{F}_2^{\text{NB}}(Q^2, \nu, t)$ at $Q^2 = 0.33 \text{ GeV}^2$ and $\theta = 150^\circ$ as function of W . Left panel: results from the subtracted DRs with the separate contributions from the s - and t -channel, and for a value of the GP combination $\alpha_{E1}(Q^2) + \beta_{M1}(Q^2) = 5.44 \times 10^{-4} \text{ fm}^3$. Middle panel: total results from subtracted DRs (solid black curve) compared with the unsubtracted DR result of [35] (dashed-dotted pink curve). Right panel: contribution to the imaginary part from the s -channel cut.

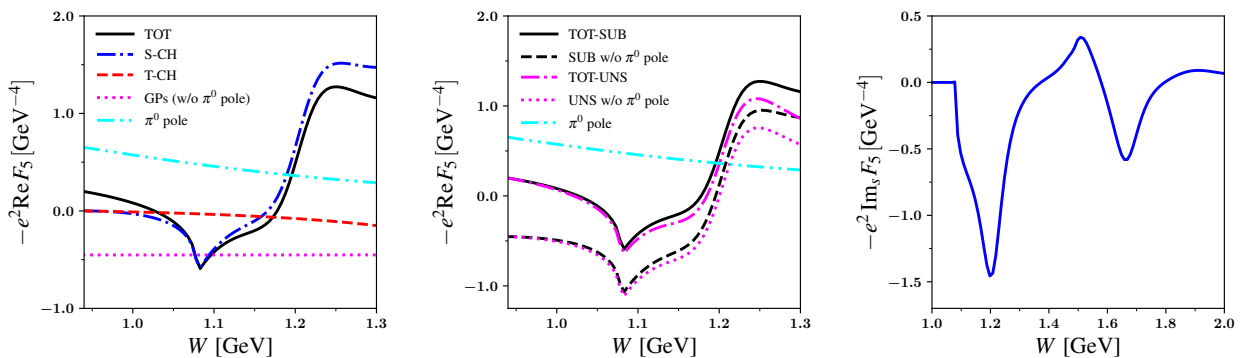


Figure 11: Real and imaginary parts of the amplitude $F_5^{\text{NB}}(Q^2, \nu, t)$ at $Q^2 = 0.33 \text{ GeV}^2$ and $\theta = 150^\circ$ as function of W . Left panel: results from the subtracted DRs, with the separate contributions from the s -channel, t -channel, π^0 pole, and GP contribution. The GP value excludes the π^0 pole contribution and is calculated according to Eq. (26) for $t = -Q^2$ and $\nu = 0$, with the upper limit of integration corresponding to $W_{\text{max}} = 2.0 \text{ GeV}$. Middle panel: comparison of the results from subtracted DRs with the unsubtracted DR result of [35], with and without the π^0 pole. Right panel: contribution to the imaginary part from the s -channel cut.

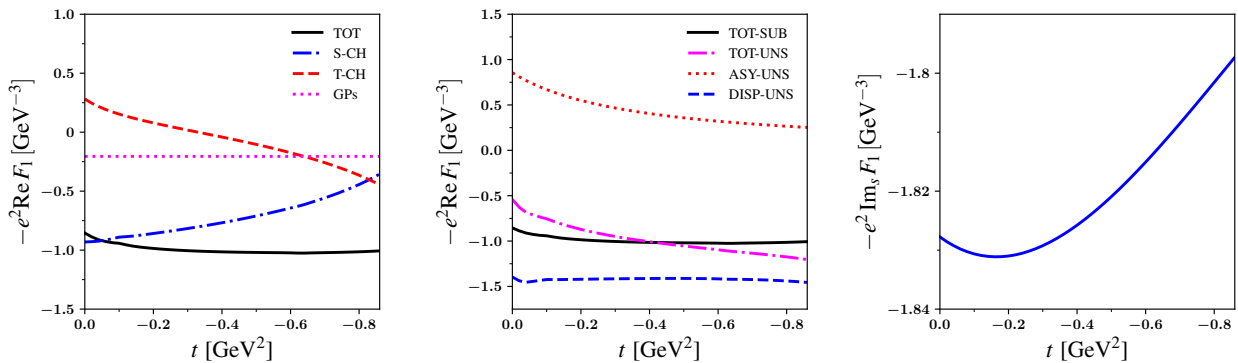


Figure 12: Real and imaginary parts of the amplitude $F_1^{\text{NB}}(Q^2, \nu, t)$ at $Q^2 = 0.33 \text{ GeV}^2$ and $W = 1.19 \text{ GeV}$ as function of t . Left panel: results from the subtracted DRs with the separate contributions from the s - and t -channel, and for a value of the GP $\beta_{M1}(Q^2) = 1.20 \times 10^{-4} \text{ fm}^3$. Middle panel: total results from subtracted DRs (solid black curve) compared with the unsubtracted DR result of [35] (dashed-dotted pink curve). For the unsubtracted DR result we also show the separate contributions of the dispersive s -channel contribution with the upper limit of integration corresponding to $W_{\text{max}} = 2.0 \text{ GeV}$ (dashed blue curve) and the asymptotic t -channel contribution (dotted red curve). Right panel: contribution to the imaginary part from the s -channel cut.

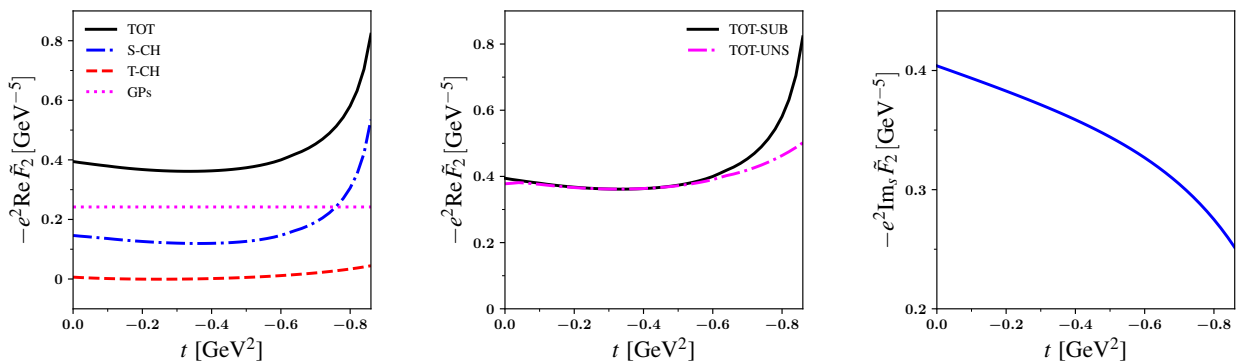


Figure 13: Real and imaginary parts of the amplitude $\tilde{F}_2^{\text{NB}}(Q^2, \nu, t)$ at $Q^2 = 0.33 \text{ GeV}^2$ and $W = 1.19 \text{ GeV}$ as function of t . Left panel: results from the subtracted DRs with the separate contributions from the s - and t -channel, and for a value of the GP combination $\alpha_{E1}(Q^2) + \beta_{M1}(Q^2) = 5.44 \times 10^{-4} \text{ fm}^3$. Middle panel: total results from subtracted DRs (solid black curve) compared with the unsubtracted DR result of [35] (dashed-dotted pink curve). Right panel: contribution to the imaginary part from the s -channel cut.

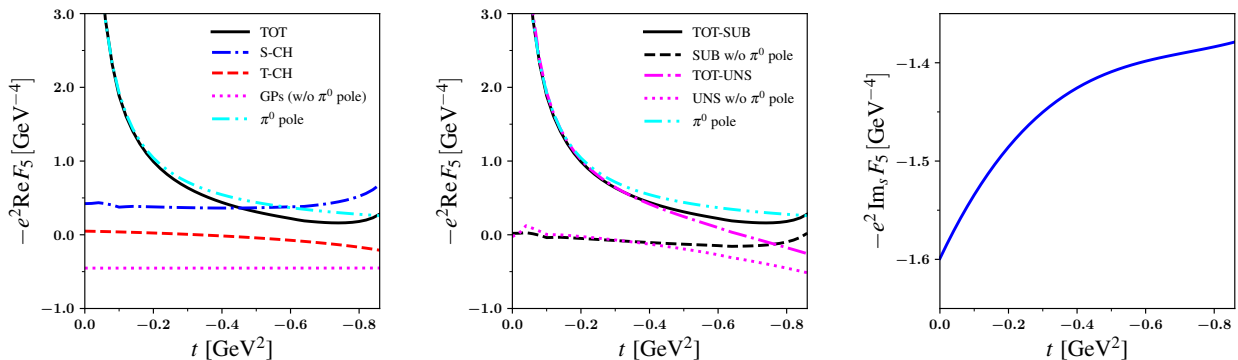


Figure 14: Real and imaginary parts of the amplitude $F_5^{\text{NB}}(Q^2, \nu, t)$ at $Q^2 = 0.33 \text{ GeV}^2$ and $W = 1.19 \text{ GeV}$ as function of t . Left panel: results from the subtracted DRs, with the separate contributions from the s -channel, t -channel, π^0 pole, and GP contribution. The GP value excludes the π^0 pole contribution and is calculated according to Eq. (26) for $t = -Q^2$ and $\nu = 0$, with the upper limit of integration corresponding to $W_{\text{max}} = 2.0 \text{ GeV}$. Middle panel: comparison of the results from subtracted DRs with the unsubtracted DR result of [35], with and without the π^0 pole. Right panel: contribution to the imaginary part from the s -channel cut.

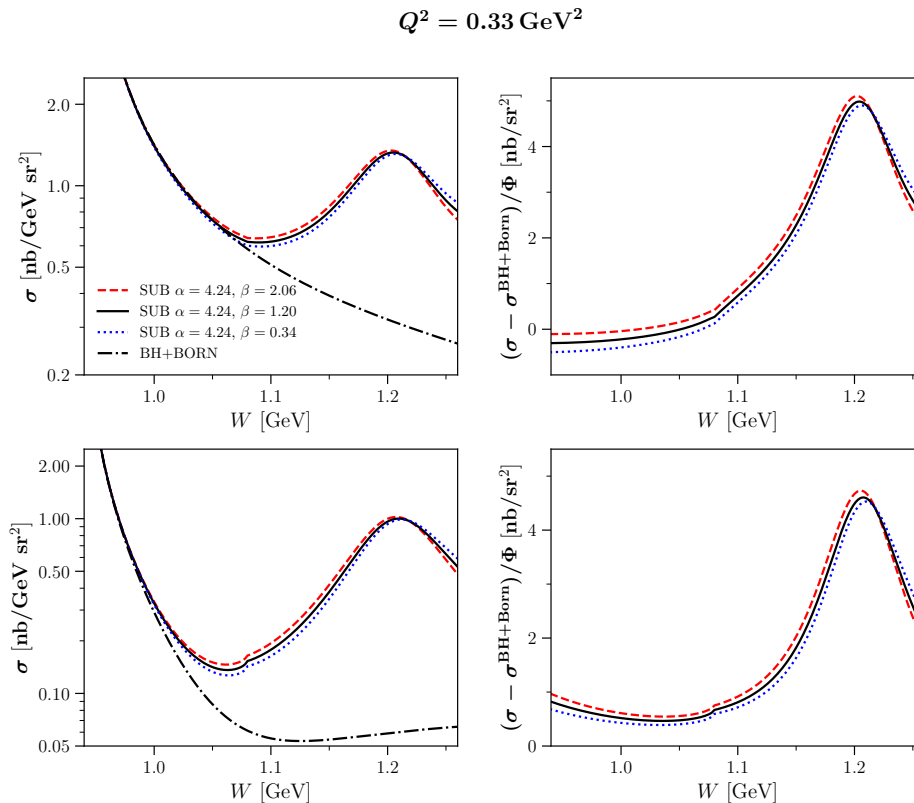


Figure 15: Left panels: $e^-p \rightarrow e^- \gamma p$ fivefold differential cross section of Eq. (46) as a function of the c.m. energy W in the kinematics of the upcoming VCS-II experiment at JLab [44]: electron beam energy $E_e = 2.2 \text{ GeV}$, initial photon virtuality $Q^2 = 0.33 \text{ GeV}^2$, and photon c.m. scattering angle $\theta = 150^\circ$. Right panels: results for $(\sigma - \sigma^{\text{BH+Born}})/\Phi$ with Φ the phase space factor, given by Eq. (47). Top and bottom panels correspond to azimuthal angle $\phi = 180^\circ$ and $\phi = 0^\circ$, respectively. The dashed-dotted curves in the left panels show the result of the BH + Born cross section. The other curves show the sensitivity in the subtracted DR formalism to the magnetic GP β_{M1} for fixed value of the electric GP α_{E1} (both in units 10^{-4} fm^3), as indicated in the legend.

amplitude in the outgoing photon c.m. energy

$$q'_{c.m.} = \frac{W^2 - M_N^2}{2W}. \quad (49)$$

In such LEX, the helicity averaged squared amplitude for the $e^-p \rightarrow e^- \gamma p$ reaction, entering Eq. (46), takes the form

$$\sum_{h,h',s,s',\lambda} |\mathcal{M}_{\text{BH}} + \mathcal{M}_{\text{VCS}}|^2 = \frac{a_{-2}}{q'_{c.m.}{}^2} + \frac{a_{-1}}{q'_{c.m.}} + a_0 + \mathcal{O}(q'_{c.m.}). \quad (50)$$

The first two coefficients in this expansion, a_{-2} and a_{-1} , are fully determined through a low-energy theorem (LET) in terms of the BH + Born amplitude, for details see [10]. The nucleon structure information, beyond the nucleon elastic form factors in the BH + Born amplitude, appears to lowest order in $q'_{c.m.}$ in the coefficient a_0 , which can be expanded in terms of dipole GPs. The unpolarized cross section contains three GP combinations,

which can be accessed by measuring the photon angular dependence and varying the beam energy. An experimental extraction of all six independent dipole GPs requires to perform also double polarization experiments involving a longitudinally polarized electron beam and either polarizing the nucleon target or measuring the nucleon recoil polarization along three orthogonal directions [54], see the review [25] for details of the formalism and the review of [26] for an overview of the low-energy VCS experiments performed so far.

We show in Fig. 15 the sensitivity of the $e^-p \rightarrow e^- \gamma p$ cross section to the GPs from threshold into the $\Delta(1232)$ -region for the kinematics of the upcoming VCS-II experiment at JLab [44]. We show the results for two values of the azimuthal angle ϕ between the lepton and hadron planes: $\phi = 0^\circ$ corresponding with the photon emitted in the same half-plane determined by the lepton beam and the scattered lepton, and $\phi = 180^\circ$ in which the photon is emitted in the opposite half-plane. One notices that in the low-energy region, below the pion produc-

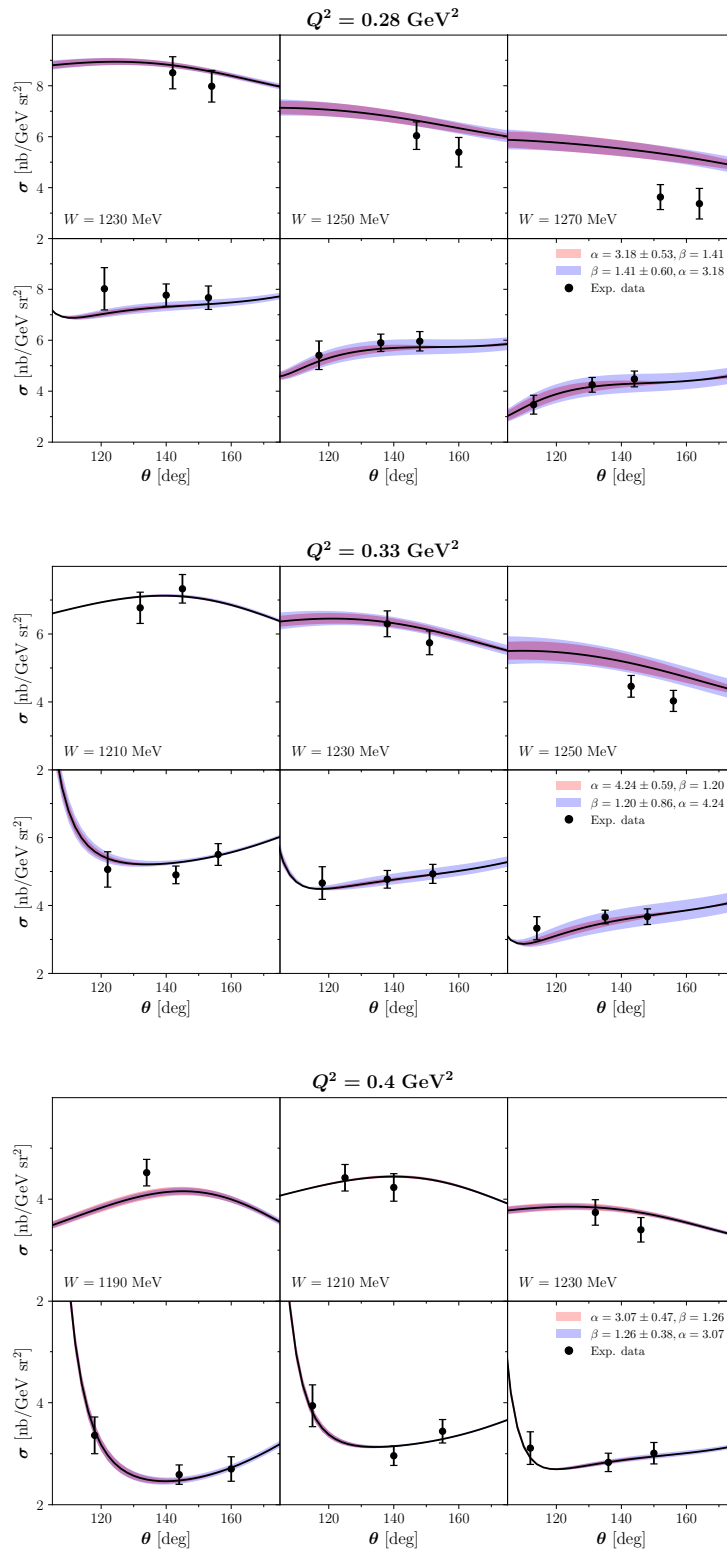


Figure 16: $e^-p \rightarrow e^-\gamma p$ fivefold differential cross section of Eq. (46) as a function of the photon c.m. scattering angle for the kinematics of the JLab experiment [24]: electron beam energy $E_e = 4.56 \text{ GeV}$, three values for photon virtuality Q^2 , and several c.m. energy W values as indicated on the panels. Top and bottom panels correspond to azimuthal angle $\phi = 180^\circ$ and $\phi = 0^\circ$, respectively. The bands show the 1σ uncertainties associated with the values of the scalar GPs extracted in Ref. [24], as indicated in the legends (all in units 10^{-4} fm^3).

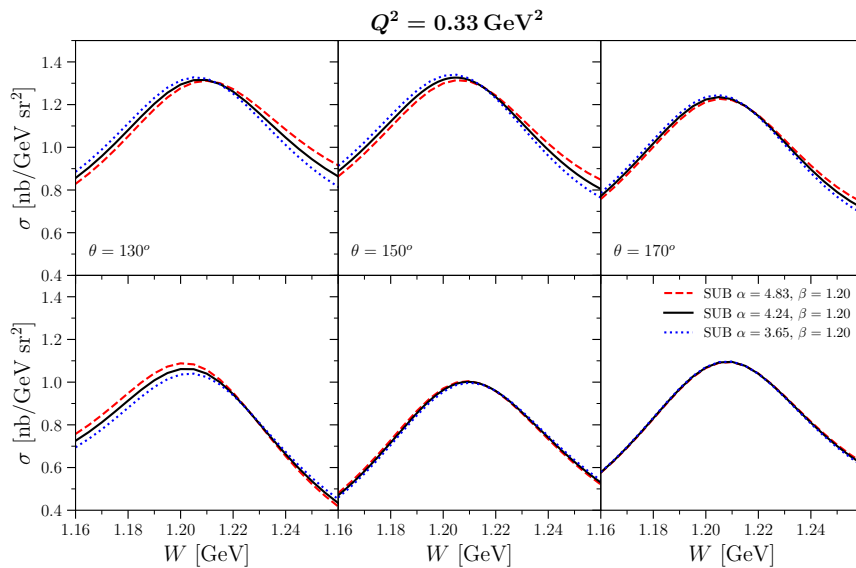


Figure 17: $e^- p \rightarrow e^- \gamma p$ fivefold differential cross section of Eq. (46) as a function of the c.m. energy W in the kinematics of the upcoming VCS-II experiment at JLab [44]: electron beam energy $E_e = 2.2$ GeV, initial photon virtuality $Q^2 = 0.33$ GeV², for several values of the photon c.m. scattering angle. Top and bottom panels correspond to azimuthal angle $\phi = 180^\circ$ and $\phi = 0^\circ$, respectively. The curves show the sensitivity to the scalar electric GP α_{E1} for fixed value of the magnetic GP β_{M1} (both in units 10^{-4} fm³), as indicated in the legend.

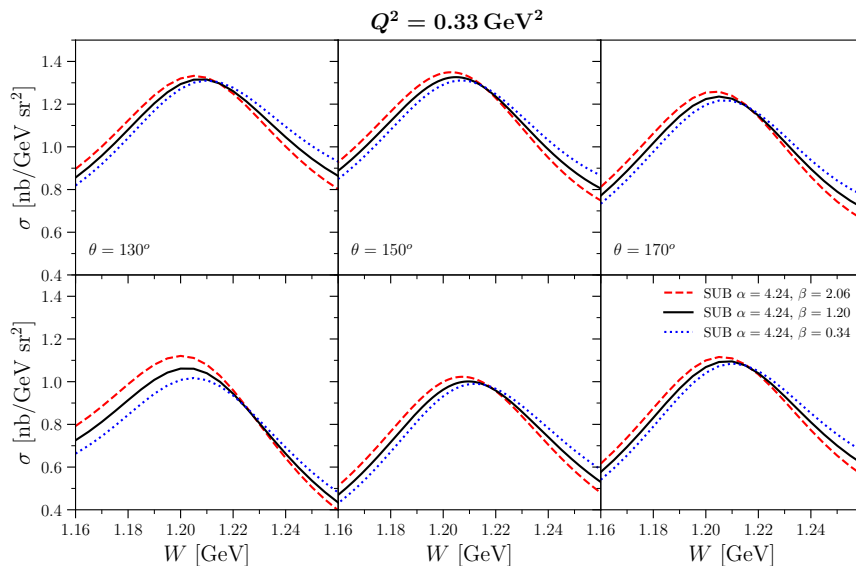


Figure 18: The same as Fig. 17, where the curves show the sensitivity to the magnetic GP β_{M1} for fixed value of the electric GP α_{E1} (both in units 10^{-4} fm³), as indicated in the legend.

tion threshold, the cross section is largely dominated by the BH+Born amplitude, in accordance with the LET, and the GPs make an effect of order 10% or less below pion production threshold. In the low-energy region, the sensitivity to the GPs arises through interference with the BH + Born amplitude. To enhance the sensitivity to the GPs, it has been proposed in [35] to measure the VCS process in the $\Delta(1232)$ region, requiring a theoretical formalism beyond the LEX of Eq. (50). For this purpose an unsubtracted dispersive formalism was developed in [35]. This formalism is improved in the present work through the largely data-driven subtracted DRs, in view of the precision goals of the present and future JLab experiments. In the subtracted DR formalism the scalar GPs directly appear as subtraction constants and are to be determined from a fit to the VCS cross sections. In the $\Delta(1232)$ region, one sees that the BH + Born process is only responsible for around 10 - 20% of the cross section, which is predominantly driven by the $\Delta(1232)$ -resonance excitation. The sensitivity to the GPs in this region therefore arises mainly through the interference with the real part of the $\Delta(1232)$ resonance amplitude. As the real part of the $\Delta(1232)$ production amplitude goes through a zero at the resonance position, where the amplitude is purely imaginary, one thus expects the largest sensitivity to the GPs on either side of the resonance peak position. As illustration, we show in Fig. 15 the sensitivity of the $e^-p \rightarrow e^- \gamma p$ cross section to a $\pm 1\sigma$ (standard deviation) variation in the magnetic dipole GP $\beta_{M1}(Q^2)$ around its value at $Q^2 = 0.33 \text{ GeV}^2$ measured at JLab [24], for the fixed value of the electric dipole GP $\alpha_{E1}(Q^2)$ measured in the same experiment.

In Fig. 16 a direct comparison between our subtracted DR formalism and the existing VCS JLab data from [24] is shown as function of the photon c.m. angle for three Q^2 values and for different W values through the $\Delta(1232)$ energy range. As the GPs $\alpha_{E1}(Q^2)$ and $\beta_{M1}(Q^2)$ at each value of Q^2 are subtraction constants in our formalism, we show as a first step the comparison using the central values extracted in [24], which were obtained using the unsubtracted DR formalism of [35]. Furthermore, in Fig. 16 we also show the sensitivity bands in α and β by considering 1σ variations around their central values. For the data at $Q^2 = 0.4 \text{ GeV}^2$, which are mostly centered near the peak of the $\Delta(1232)$, one notices that the sensitivity to the GP is reduced as the amplitude is mostly imaginary around the resonance position. This kinematics thus provides a good test of the dispersive formalism. One notices that the angular dependence is well reproduced. For the lower Q^2 values, $Q^2 = 0.28 \text{ GeV}^2$ and $Q^2 = 0.33 \text{ GeV}^2$, shown in Fig. 16, the existing data are mostly at and above the $\Delta(1232)$ peak position. Overall the subtracted DR formalism follows also well the angular distributions and the decrease of the cross section when going from the $\Delta(1232)$ peak to higher W values. Merely at the highest W bin, and for $\phi = 180^\circ$, one sees a deviation beyond the 1σ sensitivity bands for the GPs. Before drawing conclusions as whether the origin of this

deviation is caused by the GP values extracted in [24], a global fit to all world data is required. Such a fit of the scalar GPs to the world VCS data using the subtracted DR formalism is planned for a future work.

As the real part of the $\Delta(1232)$ production amplitude changes sign when crossing the resonance position, also the interference effect with the GPs on the cross section changes sign when crossing the resonance position. Therefore, a simultaneous measurement both below and above the $\Delta(1232)$ resonance position will provide strong consistency checks on the extraction of the GPs α_{E1} and β_{M1} . Such a measurement is planned in the near future at JLab [44] and will complement the existing JLab data from [24], shown in Fig. 16, which were mostly taken around or above the $\Delta(1232)$ peak position. In Figs. 17 and 18 we show the predictions of our subtracted DR formalism for the expected sensitivity to α_{E1} and β_{M1} in the kinematics of the forthcoming VCS-II experiment [44]. One clearly notices the sign change in the interference effect with the GPs when crossing the resonance position. One also notices in Fig. 17, especially for $\theta = 130^\circ$ below the resonance position, regarding the sensitivity to the GP α_{E1} there is a change in interference for azimuthal angles $\phi = 180^\circ$ and $\phi = 0^\circ$. For $\phi = 180^\circ$ our results predict an anti-correlation between the GPs α_{E1} and β_{M1} : increasing the value of α_{E1} or decreasing the value of β_{M1} affect the cross section in a similar way. On the other hand for $\phi = 0^\circ$ our results predict a correlation between the GPs α_{E1} and β_{M1} : increasing the value of α_{E1} or increasing the value of β_{M1} affect the cross section in a similar way. Thus, the forthcoming JLab measurement [44] of the photon angular dependence of the $e^-p \rightarrow e^- \gamma p$ reaction both below and above the $\Delta(1232)$ position will allow for a strong consistency check on the extraction of the GPs using the subtracted DR formalism.

In order to test the imaginary part of the VCS DR formalism, a further planned JLab VCS-IIIp experiment [45] will measure the beam spin asymmetry (BSA) of the $e^-p \rightarrow e^- \gamma p$ reaction, which is the asymmetry for reversal of the electron beam helicity h , i.e.,

$$\text{BSA} = \frac{d^5\sigma_{h=+1/2} - d^5\sigma_{h=-1/2}}{d^5\sigma_{h=+1/2} + d^5\sigma_{h=-1/2}}, \quad (51)$$

where $d^5\sigma_h$ denotes the fivefold $e^-p \rightarrow e^- \gamma p$ differential cross section for an electron beam in a pure helicity state $h = \pm 1/2$. This observable is zero below the pion production threshold, as the $e^-p \rightarrow e^- p \gamma$ amplitude is purely real in that region. Above the pion production threshold, the BSA firstly tests the dispersive input as it is sensitive to the imaginary part of the VCS amplitude. Furthermore, the numerator of the BSA in Eq. (51) has a $\sin\phi$ angular dependence. Its measurement thus requires out-of-plane kinematics. In Fig. 19, 20, we show our results for the BSA for $\phi = 45^\circ$ and $\phi = 90^\circ$. We see that the subtracted DR formalism predicts asymmetries in the range between -5% to +3% in the kinematics of the JLab VCS-IIIp experiment. Fig. 19 also illustrates

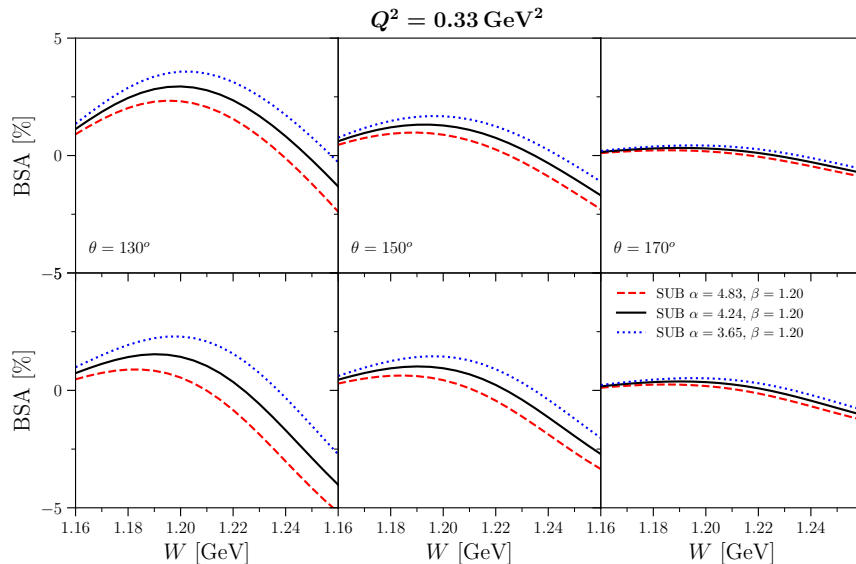


Figure 19: Beam spin asymmetry (BSA) for the $e^-p \rightarrow e^-\gamma p$ reaction as a function of the c.m. energy W in the kinematics of the planned VCS-IIIp experiment at JLab [45]: electron beam energy $E_e = 2.2$ GeV, initial photon virtuality $Q^2 = 0.33$ GeV², for several values of the photon c.m. scattering angle. Top and bottom panels correspond to azimuthal angle $\phi = 45^\circ$ and $\phi = 90^\circ$, respectively. The curves show the sensitivity to the electric GP α_{E1} for fixed value of the magnetic GP β_{M1} (both in units 10^{-4} fm³), as indicated in the legend.

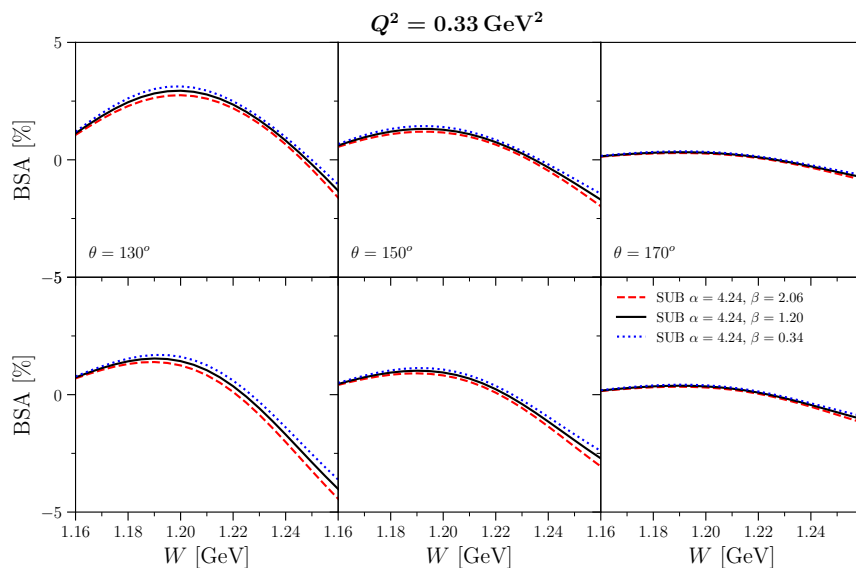


Figure 20: The same as Fig. 19, where the curves show the sensitivity to the magnetic GP β_{M1} for fixed value of the electric GP α_{E1} (both in units 10^{-4} fm³), as indicated in the legend.

that the BSA has a significant sensitivity to the GP α_{E1} especially below the $\Delta(1232)$ resonance position, while Fig. 20 shows that the BSA is nearly insensitive to the GP β_{M1} . This sensitivity to the GP α_{E1} in the BSA can be understood, as this observable results from the product of the imaginary part of the VCS amplitude for $\Delta(1232)$ production due to a transverse virtual photon

(predominantly M1 excitation) with the real part of the VCS amplitude for a longitudinal virtual photon. The latter contains the dependence on α_{E1} . The BSA thus provides a further strong cross-check on the extraction of α_{E1} from the unpolarized cross section.

V. CONCLUSIONS AND OUTLOOK

In this work we developed a once-subtracted dispersion-relation (DR) formalism for virtual Compton scattering (VCS) off the proton from threshold into the $\Delta(1232)$ region, with the aim of extracting the scalar generalized polarizabilities (GPs) with controlled input in view of the precision goals of the ongoing and forthcoming measurements at Jefferson Lab.

The central improvement over the previously used unsubtracted DR formalism is the replacement of the finite-energy sum-rule prescription and effective asymptotic parameterizations by a subtracted framework in which the relevant low-energy structure information enters through subtraction constants. In the present implementation, the VCS amplitudes for which the unsubtracted dispersion integrals are not convergent (F_1^{NB} , F_5^{NB}) or poorly convergent (\tilde{F}_2^{NB}) are reconstructed from fixed- t once-subtracted dispersion integrals in ν , while the subtraction functions are obtained from once-subtracted dispersion relations in t . This provides rapidly convergent dispersive integrals for both right-hand and left-hand cuts. The dominant t -channel dynamics are treated in a largely data-driven way through $\gamma^*\gamma \rightarrow \pi\pi$ and $\pi\pi \rightarrow N\bar{N}$ dispersive input, including the prominent $f_0(500)$ and $f_2(1270)$ regions, while the leading left-hand cut in the $\Delta(1232)$ -energy region is estimated through $\Delta(1232)$ exchange with finite width.

We presented numerical results for the subtracted amplitudes and their decomposition into s - and t -channel contributions, highlighting the modified t -dependence relative to the unsubtracted formalism, in particular for F_1^{NB} where the earlier effective $f_0(500)$ pole approximation is replaced by an explicit dispersive evaluation. In the s -channel, the dispersive integrals entering the subtracted relations are largely saturated by the low-energy region up to and around the $\Delta(1232)$, which is essential for a quantitatively reliable description of the W dependence in the resonance region.

Confronting the formalism with the latest VCS cross-section data in the $\Delta(1232)$ region, we find an overall good description of the angular distributions and of the observed decrease of the cross section with increasing W . A deviation appears only in the highest- W bin for $\phi = 180^\circ$, where the data lie outside the sensitivity band obtained from the scalar GPs as extracted in the previous analysis. Establishing whether this indicates tension in the polarizability input or points to missing contributions requires a global analysis of the world data set within the present subtracted framework, which we plan to pursue in future work.

The subtracted DR formalism also yields clear expectations for forthcoming measurements designed to test both the real and imaginary parts of the VCS amplitude in the Δ region. Since the sensitivity to the scalar GPs $\alpha_{E1}(Q^2)$ and $\beta_{M1}(Q^2)$ is driven by interference with the real part of the $\Delta(1232)$ amplitude, the largest impact of the scalar GPs occurs on either side of the resonance

peak, while it is reduced close to the peak where the amplitude is predominantly imaginary. For the planned kinematics of the VCS-II experiment at JLab, the predicted dependence on the azimuthal angle ϕ implies that measurements at $\phi = 0^\circ$ and $\phi = 180^\circ$, taken below and above the resonance, provide strong internal consistency checks and show different correlation patterns between α_{E1} and β_{M1} .

A complementary constraint will come from polarization observables. In particular, the beam-spin asymmetry above pion threshold directly tests the dispersive input through its sensitivity to the imaginary part of the VCS amplitude. For the planned kinematics of the VCS-IIIp experiment at JLab we predict asymmetries at the few-percent level and a pronounced sensitivity to α_{E1} below the $\Delta(1232)$, while the dependence on β_{M1} is much weaker, providing an independent cross-check on the extraction of α_{E1} from unpolarized cross sections.

Looking ahead, several extensions are natural. On the phenomenological side, a global fit of $\alpha_{E1}(Q^2)$ and $\beta_{M1}(Q^2)$ to the full set of VCS cross section data, including a consistent propagation of uncertainties from the pion electroproduction input and from the t -channel dispersive amplitudes, will be essential to fully exploit the precision of current and upcoming measurements. On the theory side, the treatment of the t -channel left-hand cut can be further refined by incorporating contributions beyond the leading $\Delta(1232)$ exchange, and the t -channel right-hand-cut input can be improved by including the $f_0(980)$ in a coupled-channel framework. Finally, combining the present framework with dedicated double-polarization measurements offers a path toward a dispersive extraction of the spin GPs, thereby extending the reach of the subtracted DR approach beyond the scalar sector.

Acknowledgements

This work was supported by the Deutsche Forschungsgemeinschaft (DFG, German Research Foundation), in part through the Collaborative Research Center (CRC1660: Hadron and Nuclei as discovery tools – Project ID 514321794), and in part through the Cluster of Excellence (Precision Physics, Fundamental Interactions, and Structure of Matter) (PRISMA⁺ EXC 2118/1) within the German Excellence Strategy (Project ID 39083149).

Appendix A: t -channel helicity amplitudes for VCS

The t -channel helicity amplitudes for virtual Compton scattering, corresponding with the $\gamma\gamma^* \rightarrow N\bar{N}$ process,

can be written as

$$T_{\lambda_1, \lambda_2, \lambda_N, \lambda_{\bar{N}}}^t = -e^2 \varepsilon_2^\mu(q_2, \lambda_2) \varepsilon_1^\nu(q_1, \lambda_1) \times \bar{u}(p_1, \lambda_N) \tilde{\mathcal{M}}_{\mu\nu} v(p_2, \lambda_{\bar{N}}), \quad (\text{A1})$$

where ε_2 and ε_1 are the polarization vectors of the virtual and real photon respectively, and u and v are the Dirac spinors of the nucleon and antinucleon in the final state. The tensor $\tilde{\mathcal{M}}_{\mu\nu}$ has the following definition:

$$\tilde{\mathcal{M}}_{\mu\nu} = \sum_{i=1}^{12} f_i(Q^2, \nu, t) \tilde{\rho}_{\mu\nu}^i, \quad (\text{A2})$$

where the gauge-invariant tensor basis $\tilde{\rho}_{\mu\nu}^i$ coincides with the basis introduced in Appendix A of [35], but with the following crossing transformation (combined with a change of notation):

$$q \rightarrow q_2, \quad p \rightarrow -p_2, \quad q' \rightarrow -q_1, \quad p' \rightarrow p_1. \quad (\text{A3})$$

The f_i are the same invariant amplitudes as in Eq. (7). In this Appendix, we express the invariant amplitudes F_i in terms of these t -channel helicity amplitudes. As expected, the number of independent helicity amplitudes matches the number of twelve independent invariant amplitudes. We choose the following set of independent helicity amplitudes: the polarization of the antinucleon is fixed at $1/2$, while the polarizations of the other particles are varied, leading to the following independent amplitudes

$$\begin{aligned} & T_{1,1,\frac{1}{2},\frac{1}{2}}^t, \quad T_{-1,-1,\frac{1}{2},\frac{1}{2}}^t, \quad T_{1,1,-\frac{1}{2},\frac{1}{2}}^t, \\ & T_{-1,-1,-\frac{1}{2},\frac{1}{2}}^t, \quad T_{1,0,\frac{1}{2},\frac{1}{2}}^t, \quad T_{-1,0,\frac{1}{2},\frac{1}{2}}^t, \\ & T_{1,0,-\frac{1}{2},\frac{1}{2}}^t, \quad T_{-1,0,-\frac{1}{2},\frac{1}{2}}^t, \quad T_{1,-1,\frac{1}{2},\frac{1}{2}}^t, \\ & T_{-1,1,\frac{1}{2},\frac{1}{2}}^t, \quad T_{1,-1,-\frac{1}{2},\frac{1}{2}}^t, \quad T_{-1,1,-\frac{1}{2},\frac{1}{2}}^t. \end{aligned} \quad (\text{A4})$$

In order to find the relations with the invariant amplitudes F_i , as a first step, we implement the helicity amplitude for the t -channel of VCS of Eq. (A1). We work in the c.m. system of the t -channel process $\gamma\gamma^* \rightarrow N\bar{N}$ (see Fig. 21 for the kinematics). In this frame, the four-momenta are defined as

$$q_1^\mu = (q_{cm}, 0, 0, q_{cm}), \quad (\text{A5})$$

$$q_2^\mu = (E_q, 0, 0, -q_{cm}), \quad (\text{A6})$$

$$p_1^\mu = (E_N, p_N \sin \theta_t, 0, p_N \cos \theta_t), \quad (\text{A7})$$

$$p_2^\mu = (E_N, -p_N \sin \theta_t, 0, -p_N \cos \theta_t). \quad (\text{A8})$$

In the following, for simplicity, θ_t will be denoted by θ . The energies and the magnitudes of the three-momenta in Eqs. (A5)-(A8) can be expressed in terms of the Mandelstam variables as

$$\begin{aligned} q_{cm} &= \frac{t + Q^2}{2\sqrt{t}}, \quad E_q = \frac{t - Q^2}{2\sqrt{t}}, \\ E_N &= \frac{\sqrt{t}}{2}, \quad p_N = \sqrt{\frac{t}{4} - M_N^2}. \end{aligned} \quad (\text{A9})$$

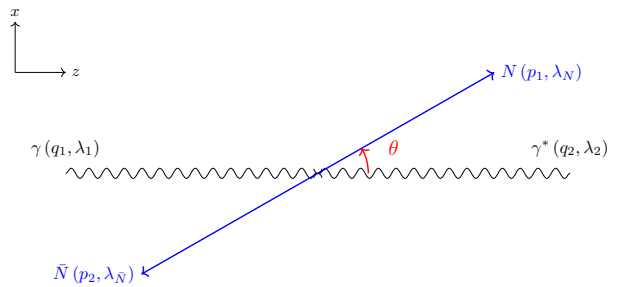


Figure 21: The kinematics of the $\gamma\gamma^* \rightarrow N\bar{N}$ process in the c.m. frame.

We use the Lorenz gauge for the photon polarization vectors. For the real photon they are given by

$$\begin{aligned} \varepsilon_1^\mu(q_1, \lambda_1 = 1) &= \frac{1}{\sqrt{2}}(0, -1, -i, 0), \\ \varepsilon_1^\mu(q_1, \lambda_1 = -1) &= \frac{1}{\sqrt{2}}(0, 1, -i, 0), \end{aligned} \quad (\text{A10})$$

whereas for the virtual photon, the polarization vectors read

$$\begin{aligned} \varepsilon_2^\mu(q_2, \lambda_2 = 1) &= \frac{1}{\sqrt{2}}(0, 1, -i, 0), \\ \varepsilon_2^\mu(q_2, \lambda_2 = -1) &= \frac{1}{\sqrt{2}}(0, -1, -i, 0), \\ \varepsilon_2^\mu(q_2, \lambda_2 = 0) &= \frac{1}{Q}(-q_{cm}, 0, 0, E_q). \end{aligned} \quad (\text{A11})$$

The spinor conventions for the nucleon and the antinucleon in the final state characterized, respectively, by momenta \vec{p}_1 and \vec{p}_2 and by polarizations λ_N and $\lambda_{\bar{N}}$ are

$$\begin{aligned} u(\vec{p}_1, \lambda_N = 1/2) &= \sqrt{E_N + M_N} \begin{bmatrix} \chi_\uparrow(\theta) \\ \frac{p_N}{E_N + M_N} \chi_\uparrow(\theta) \end{bmatrix}, \\ u(\vec{p}_1, \lambda_N = -1/2) &= \sqrt{E_N + M_N} \begin{bmatrix} \chi_\downarrow(\theta) \\ -\frac{p_N}{E_N + M_N} \chi_\downarrow(\theta) \end{bmatrix}, \end{aligned} \quad (\text{A12})$$

and

$$\begin{aligned} v(\vec{p}_2, \lambda_{\bar{N}} = 1/2) &= \sqrt{E_N + M_N} \begin{bmatrix} -\frac{p_N}{E_N + M_N} \chi'_\downarrow(\theta) \\ \chi'_\downarrow(\theta) \end{bmatrix}, \\ v(\vec{p}_2, \lambda_{\bar{N}} = -1/2) &= \sqrt{E_N + M_N} \begin{bmatrix} -\frac{p_N}{E_N + M_N} \chi'_\uparrow(\theta) \\ -\chi'_\uparrow(\theta) \end{bmatrix}, \end{aligned} \quad (\text{A13})$$

where

$$\begin{aligned} \chi_\uparrow(\theta) &= \begin{bmatrix} \cos \theta/2 \\ \sin \theta/2 \end{bmatrix}, \quad \chi_\downarrow(\theta) = \begin{bmatrix} -\sin \theta/2 \\ \cos \theta/2 \end{bmatrix}, \\ \chi'_\uparrow(\theta) &= \begin{bmatrix} \sin \theta/2 \\ -\cos \theta/2 \end{bmatrix}, \quad \chi'_\downarrow(\theta) = \begin{bmatrix} \cos \theta/2 \\ \sin \theta/2 \end{bmatrix}. \end{aligned} \quad (\text{A14})$$

The relations between the independent t -channel helicity amplitudes and VCS invariant amplitudes can be written

in matrix form as

$$\vec{T}^t = \tilde{A}_1 \vec{F}, \quad (\text{A15})$$

where \tilde{A}_1 is a 12×12 matrix, \vec{F} is a vector whose components are the VCS invariant amplitudes F_i , and \vec{T}^t is the vector containing the independent t -channel helicity amplitudes listed in Eqs. (A4). By inverting the matrix \tilde{A}_1 , we can express the VCS invariant amplitudes in terms of the t -channel helicity amplitudes.

Furthermore, it is useful to introduce reduced VCS t -channel helicity amplitudes τ_i , $i = 1, \dots, 12$, defined by the following relations:

$$\begin{aligned} T_{1,1,\frac{1}{2},\frac{1}{2}}^t &= \tau_1^t \\ T_{-1,-1,\frac{1}{2},\frac{1}{2}}^t &= \tau_2^t \\ T_{1,1,-\frac{1}{2},\frac{1}{2}}^t &= \sin\left(\frac{\theta}{2}\right) \cos\left(\frac{\theta}{2}\right) \tau_3^t \end{aligned}$$

$$\begin{aligned} T_{-1,-1,-\frac{1}{2},\frac{1}{2}}^t &= \sin\left(\frac{\theta}{2}\right) \cos\left(\frac{\theta}{2}\right) \tau_4^t \\ T_{1,-1,\frac{1}{2},\frac{1}{2}}^t &= \sin^2\left(\frac{\theta}{2}\right) \cos^2\left(\frac{\theta}{2}\right) \tau_5^t \\ T_{-1,1,\frac{1}{2},\frac{1}{2}}^t &= \sin^2\left(\frac{\theta}{2}\right) \cos^2\left(\frac{\theta}{2}\right) \tau_6^t \\ T_{1,-1,-\frac{1}{2},\frac{1}{2}}^t &= \sin^3\left(\frac{\theta}{2}\right) \cos\left(\frac{\theta}{2}\right) \tau_7^t \\ T_{-1,1,-\frac{1}{2},\frac{1}{2}}^t &= \sin\left(\frac{\theta}{2}\right) \cos^3\left(\frac{\theta}{2}\right) \tau_8^t \\ T_{1,0,\frac{1}{2},\frac{1}{2}}^t &= \sin\left(\frac{\theta}{2}\right) \cos\left(\frac{\theta}{2}\right) \tau_9^t \\ T_{-1,0,\frac{1}{2},\frac{1}{2}}^t &= \sin\left(\frac{\theta}{2}\right) \cos\left(\frac{\theta}{2}\right) \tau_{10}^t \\ T_{1,0,-\frac{1}{2},\frac{1}{2}}^t &= \sin^2\left(\frac{\theta}{2}\right) \tau_{11}^t \\ T_{-1,0,-\frac{1}{2},\frac{1}{2}}^t &= \cos^2\left(\frac{\theta}{2}\right) \tau_{12}^t. \end{aligned} \quad (\text{A16})$$

In terms of the t -channel reduced helicity amplitudes τ_i^t of Eq. (A16), the VCS invariant amplitudes $F_i(Q^2, \nu, t)$ read

$$-e^2 F_1 = \frac{1}{(t - 4M_N^2)^{1/2} (Q^2 + t)} \left[-(\tau_1^t + \tau_2^t) - \frac{1}{4} (\tau_5^t + \tau_6^t) \right] \quad (\text{A17})$$

$$+ \frac{16\nu^2 Q^2 M_N}{(Q^2 + t)^3 (t - 4M_N^2)^{3/2}} \left[M_N (\tau_5^t + \tau_6^t) + \frac{\sqrt{t}}{2} (\tau_7^t - \tau_8^t) \right]$$

$$- \frac{2\nu}{(Q^2 + t)^2 (t - 4M_N^2)} \left[t (\tau_3^t + \tau_4^t) - \frac{t}{2} (\tau_7^t + \tau_8^t) + 2\sqrt{2} Q M_N (\tau_9^t - \tau_{10}^t) + \sqrt{2} Q \sqrt{t} (\tau_{11}^t + \tau_{12}^t) \right],$$

$$-e^2 F_2 = \frac{1}{(t - 4M_N^2)^{3/2} (Q^2 + t)} \frac{1}{2} \left\{ -(\tau_5^t + \tau_6^t) - \frac{\sqrt{t}}{2M_N} (\tau_7^t - \tau_8^t) \right\}, \quad (\text{A18})$$

$$-e^2 F_3 = \frac{2M_N}{(t - 4M_N^2)^{3/2} (Q^2 + t)^2} \left\{ (\tau_5^t + \tau_6^t) + \frac{\sqrt{t}}{2M_N} (\tau_7^t - \tau_8^t) \right\} \quad (\text{A19})$$

$$- \frac{1}{2\sqrt{2} (t - 4M_N^2) (Q^2 + t) Q \nu} \left[(\tau_9^t - \tau_{10}^t) + \frac{\sqrt{t}}{2M_N} (\tau_{11}^t + \tau_{12}^t) \right],$$

$$-e^2 F_4 = - \frac{1}{8\nu (t - 4M_N^2) (Q^2 + t)} (\tau_7^t + \tau_8^t), \quad (\text{A20})$$

$$-e^2 F_5 = \frac{1}{(Q^2 + t)} \frac{1}{M_N \sqrt{t}} \left\{ -(\tau_1^t - \tau_2^t) + \frac{M_N^2 (Q^4 + 16\nu^2 Q^2 + 2Q^2 t + t^2)}{(t - 4M_N^2) (Q^2 + t)^2} (\tau_5^t - \tau_6^t) \right.$$

$$- \frac{4\sqrt{2} M_N Q \nu}{(t - 4M_N^2)^{1/2} (Q^2 + t)} (\tau_9^t + \tau_{10}^t) - \frac{8\nu^2 M_N Q^2}{(Q^2 + t)^2} (\tau_7^t - \tau_8^t)$$

$$\left. + \frac{1}{(t - 4M_N^2)^{1/2}} \left[-M_N \left[(\tau_3^t - \tau_4^t) + \frac{1}{2} (\tau_7^t - \tau_8^t) - \frac{\sqrt{2t}}{Q} (\tau_{11}^t - \tau_{12}^t) \right] \right] \right\}, \quad (\text{A21})$$

$$+ \frac{2\nu (t - 4M_N^2)^{1/2}}{(Q^2 + t)} \left[\sqrt{t} (\tau_3^t + \tau_4^t) - \sqrt{t} \frac{8M_N - t}{2(t - 4M_N^2)} (\tau_7^t + \tau_8^t) + \sqrt{2} Q (\tau_{11}^t + \tau_{12}^t) \right] \left. \right\},$$

$$-e^2 F_6 = \frac{1}{8M_N \sqrt{t} (t - 4M_N^2)^{1/2} (Q^2 + t)^3} \left\{ \left[((Q^2 + t)^2 + Q^4) (\tau_7^t - \tau_8^t) - \frac{4M_N Q^2 (Q^2 + t)}{(t - 4M_N^2)^{1/2}} (\tau_5^t - \tau_6^t) \right] \right.$$

$$- \frac{Q^2 (t - 4M_N^2)^{1/2} (Q^2 + t)}{8M_N \nu} \left[2\sqrt{t} (\tau_3^t + \tau_4^t) + \sqrt{t} (\tau_7^t + \tau_8^t) + 2\sqrt{2} Q (\tau_{11}^t + \tau_{12}^t) \right] \quad (\text{A22})$$

$$\left. + \frac{Q (Q^2 + t)^2}{\sqrt{2}\nu} (\tau_9^t + \tau_{10}^t) \right\}, \quad (\text{A23})$$

$$\begin{aligned}
-e^2 F_7 = & + \frac{\sqrt{t}}{(t-4M_N^2)^{1/2}(Q^2+t)^2} (\tau_3^t - \tau_4^t) + \frac{M_N}{\sqrt{t}(t-4M_N^2)(Q^2+t)} (\tau_5^t - \tau_6^t) \\
& - \frac{Q^2}{2\sqrt{t}(t-4M_N^2)^{1/2}(Q^2+t)^2} (\tau_7^t - \tau_8^t) - \frac{4M_N Q^2 \nu}{(t-4M_N^2)(Q^2+t)^3} (\tau_7^t + \tau_8^t) \\
& + \frac{\sqrt{2}Q}{(t-4M_N^2)^{1/2}(Q^2+t)^2} (\tau_{11}^t - \tau_{12}^t), \tag{A24}
\end{aligned}$$

$$\begin{aligned}
-e^2 F_8 = & - \frac{4M_N}{\sqrt{t}(t-4M_N^2)(Q^2+t)^2} (\tau_5^t - \tau_6^t) + \frac{2}{\sqrt{t}(t-4M_N^2)^{1/2}(Q^2+t)^2} (\tau_7^t - \tau_8^t) \\
& + \frac{1}{2\sqrt{2}\sqrt{t}M_N Q (Q^2+t)\nu} \left[\frac{2M_N}{(t-4M_N^2)^{1/2}} (\tau_9^t + \tau_{10}^t) - (\tau_{11}^t + \tau_{12}^t) \right], \tag{A25}
\end{aligned}$$

$$\begin{aligned}
-e^2 F_9 = & - \frac{(t-Q^2)}{2\sqrt{t}(t-4M_N^2)(Q^2+t)^2} (\tau_5^t - \tau_6^t) - \frac{Q^4}{4M_N\sqrt{t}(t-4M_N^2)^{1/2}(Q^2+t)^3} (\tau_7^t - \tau_8^t) \\
& + \frac{Q^2}{16M_N^2(Q^2+t)^2\nu} \left[(\tau_3^t + \tau_4^t) + \frac{1}{2} (\tau_7^t + \tau_8^t) + \frac{Q\sqrt{2}}{\sqrt{t}} (\tau_{11}^t + \tau_{12}^t) \right. \\
& \left. - \frac{\sqrt{2}(Q^2+t)2M_N}{Q\sqrt{t}(t-4M_N^2)^{1/2}} (\tau_9^t + \tau_{10}^t) \right], \tag{A26}
\end{aligned}$$

$$-e^2 F_{10} = - \frac{1}{16M_N(Q^2+t)\nu} \left[(\tau_3^t + \tau_4^t) + \frac{1}{2} (\tau_7^t + \tau_8^t) \right] + \frac{\sqrt{t}}{4(t-4M_N^2)^{1/2}(Q^2+t)^2} (\tau_7^t - \tau_8^t), \tag{A27}$$

$$\begin{aligned}
-e^2 F_{11} = & + \frac{1}{4M_N\sqrt{t}(Q^2+t)} (\tau_1^t - \tau_2^t) - \frac{\sqrt{t}}{8(t-4M_N^2)^{1/2}(Q^2+t)^2} (\tau_7^t - \tau_8^t) \\
& + \frac{Q^2}{4\sqrt{t}(t-4M_N^2)^{1/2}(Q^2+t)^2} (\tau_3^t - \tau_4^t) - \frac{Q}{2\sqrt{2}(t-4M_N^2)^{1/2}(Q^2+t)^2} (\tau_{11}^t - \tau_{12}^t) \\
& + \frac{2Q^2\nu^2}{\sqrt{t}(t-4M_N^2)(Q^2+t)^3} \left[(t-4M_N^2)^{1/2} (\tau_7^t - \tau_8^t) - 2M_N (\tau_5^t - \tau_6^t) \right] \\
& - \frac{\nu}{4M_N(t-4M_N^2)(Q^2+t)^3} \left[(t(Q^2+t) - 4M_N^2 Q^2) (\tau_7^t + \tau_8^t) - \frac{2\sqrt{2}Q(4M_N^2 - t)}{\sqrt{t}} (\tau_{11}^t + \tau_{12}^t) \right] \\
& - \frac{\nu}{2M_N(t-4M_N^2)^{1/2}(Q^2+t)^2} \left[(t-4M_N^2)^{1/2} (\tau_3^t + \tau_4^t) - 2QM_N\sqrt{2} (\tau_9^t + \tau_{10}^t) \right], \tag{A28}
\end{aligned}$$

$$\begin{aligned}
-e^2 F_{12} = & + \frac{1}{2\sqrt{t}(t-4M_N^2)(Q^2+t)} (\tau_5^t - \tau_6^t) - \frac{Q^2}{4M_N\sqrt{t}(t-4M_N^2)^{1/2}(Q^2+t)^2} (\tau_7^t - \tau_8^t) \\
& + \frac{1}{16M_N^2(Q^2+t)\nu} \left[(\tau_3^t + \tau_4^t) + \frac{1}{2} (\tau_7^t + \tau_8^t) + \frac{\sqrt{2}Q}{\sqrt{t}} (\tau_{11}^t + \tau_{12}^t) \right] \\
& - \frac{1}{4\sqrt{2}\sqrt{t}M_N Q (t-4M_N^2)^{1/2}\nu} (\tau_9^t + \tau_{10}^t). \tag{A30}
\end{aligned}$$

As a consistency check, the RCS limit was considered. In this limit, the expressions for the invariant amplitudes given in Eqs. (A17)–(A30) were found to be consistent with the known relations between the L'vov amplitudes A_i and the t -channel helicity amplitudes for RCS (Eqs. (B3) of Ref. [32]).

Appendix B: VCS t -channel discontinuities from the $\pi\pi$ intermediate state

In the subtracted dispersion relation of Eq. (28), the t -channel integration is taken along the line $\nu = 0$. Consequently, we need the t -channel discontinuities $\text{Im}_t F_i(Q^2, \nu = 0, t)$. We evaluate the $\pi\pi$ contribution by inserting the $\pi\pi$ intermediate state into the t -channel unitarity relation and expressing the result in terms of helicity partial waves for $\gamma\gamma^* \rightarrow \pi\pi$ and $\pi\pi \rightarrow N\bar{N}$.

We first write the partial-wave expansion of the t -

channel VCS helicity amplitudes $\gamma(q_1, \lambda_1) \gamma^*(q_2, \lambda_2) \rightarrow N(\lambda_N) \bar{N}(\lambda_{\bar{N}})$ as

$$T_{\lambda_1 \lambda_2 \lambda_N \lambda_{\bar{N}}}^t = \sum_J \frac{(2J+1)}{2} T_{\lambda_1 \lambda_2 \lambda_N \lambda_{\bar{N}}}^J(t, Q^2) d_{\Lambda_N \Lambda_\gamma}^J(\theta), \quad (\text{B1})$$

where $d_{mm'}^J(\theta)$ are Wigner d -functions, and the helicity differences Λ_γ and Λ_N are defined as

$$\Lambda_\gamma \equiv \lambda_1 - \lambda_2, \quad \Lambda_N \equiv \lambda_N - \lambda_{\bar{N}}. \quad (\text{B2})$$

The helicity amplitude for $\gamma\gamma^* \rightarrow \pi\pi$ satisfies the partial-wave expansion [40, 42]

$$T_{\Lambda_\gamma}^{\gamma\gamma^* \rightarrow \pi\pi} = \sum_{J \text{ even}} (2J+1) h_{\lambda_1 \lambda_2}^J(t, Q^2) d_{\Lambda_\gamma 0}^J(\theta_{\pi\pi}), \quad (\text{B3})$$

with $\theta_{\pi\pi}$ the c.m. angle of the $\gamma\gamma^* \rightarrow \pi\pi$ process. Finally, for $\pi\pi \rightarrow N\bar{N}$ we similarly write

$$T_{\lambda_N \lambda_{\bar{N}}}^{\pi\pi \rightarrow N\bar{N}} = \sum_J \frac{(2J+1)}{2} T_{\lambda_N \lambda_{\bar{N}}}^J(t) d_{0, \Lambda_N}^J(\Theta), \quad (\text{B4})$$

where Θ denotes the c.m. angle of the $\pi\pi \rightarrow N\bar{N}$ reaction. Isospin conservation and Bose symmetry restrict the $\pi\pi$ intermediate state to $I = 0$ and even J . The $\pi\pi$ contribution to the t -channel discontinuity is obtained from the unitarity relation, which for fixed J takes the form

$$2 \text{Im} T_{\lambda_1 \lambda_2, \lambda_N \lambda_{\bar{N}}}^J(t, Q^2) = S \frac{\beta_\pi(t)}{8\pi} h_{\lambda_1 \lambda_2}^J(t, Q^2) \times \left(T_{\lambda_N \lambda_{\bar{N}}}^J(t) \right)^*, \quad (\text{B5})$$

where $\beta_\pi(t)$ is defined in Eq. (42). For the isospin-0 $\pi\pi$ intermediate state considered here, one has the symmetry factor $S = 1/2$. Parity invariance implies that

$$h_{\lambda_1 \lambda_2}^J(t) = h_{-\lambda_1, -\lambda_2}^J(t), \quad T_{-\lambda_N, -\lambda_{\bar{N}}}^J(t) = -T_{\lambda_N, \lambda_{\bar{N}}}^J(t), \quad (\text{B6})$$

so that the independent amplitudes may be labeled by $\Lambda_\gamma = 0, 1, 2$ and $\Lambda_N = 0, 1$. We therefore introduce the shorthand notations

$$h_{\Lambda_\gamma}^J(t), \quad T_{\Lambda_N}^J(t), \quad (\text{B7})$$

with $T_{\Lambda_N=0}^J \equiv T_{\frac{1}{2}\frac{1}{2}}^J$. Using Eq. (B1) together with Eq. (B5), and truncating the $\pi\pi$ system to $J = 0, 2$, one obtains the following relations for the imaginary part of the reduced t -channel helicity amplitudes τ_i^t (defined in Appendix A):

$$\begin{aligned} \text{Im}\tau_1^t = \text{Im}\tau_2^t &= \frac{\beta_\pi(t)}{64\pi} \left[h_0^0(t, Q^2) (T_0^0(t))^* \right. \\ &\quad \left. + \frac{5}{4}(1 + 3 \cos 2\theta) h_0^2(t, Q^2) (T_0^2(t))^* \right], \\ \text{Im}\tau_3^t = \text{Im}\tau_4^t &= -\frac{5\sqrt{6}\beta_\pi(t)}{64\pi} \cos \theta h_0^2(t, Q^2) (T_1^2(t))^*, \\ \text{Im}\tau_5^t = \text{Im}\tau_6^t &= \frac{5\sqrt{6}\beta_\pi(t)}{64\pi} h_2^2(t, Q^2) (T_0^2(t))^*, \\ \text{Im}\tau_7^t = -\text{Im}\tau_8^t &= -\frac{5\beta_\pi(t)}{32\pi} h_2^2(t, Q^2) (T_1^2(t))^*, \\ \text{Im}\tau_9^t = -\text{Im}\tau_{10}^t &= \frac{5\sqrt{6}\beta_\pi(t)}{64\pi} \cos \theta h_1^2(t, Q^2) (T_0^2(t))^*, \\ \text{Im}\tau_{11}^t &= -\frac{5\beta_\pi(t)}{64\pi} (1 + 2 \cos \theta) h_1^2(t, Q^2) (T_1^2(t))^*, \\ \text{Im}\tau_{12}^t &= -\frac{5\beta_\pi(t)}{64\pi} (-1 + 2 \cos \theta) h_1^2(t, Q^2) (T_1^2(t))^*. \end{aligned} \quad (\text{B8})$$

For the reaction $\pi\pi \rightarrow N\bar{N}$ we express the partial waves $T_{\Lambda_N}^J(t)$ through the Frazer-Fulco amplitudes $f_\pm^J(t)$ [51] as

$$\begin{aligned} T_0^J(t) &= \frac{16\pi}{p_N} (p_N p_\pi)^J f_+^J(t), \\ T_1^J(t) &= \frac{8\pi\sqrt{t}}{p_N} (p_N p_\pi)^J f_-^J(t), \end{aligned} \quad (\text{B9})$$

with the c.m. momenta

$$p_\pi = \frac{\sqrt{t}}{2} \beta_\pi, \quad p_N = \sqrt{\frac{t}{4} - M_N^2}. \quad (\text{B10})$$

Combining the above relations with the definitions of the invariant amplitudes in Appendix A, we obtain

$$\begin{aligned} -e^2 \text{Im}_t F_1(Q^2, 0, t) &= \frac{\beta_\pi}{(t+Q^2)} \left\{ \frac{1}{(4M_N^2-t)} h_0^0(t, Q^2) f_+^{0*}(t) + \frac{5}{32} t \beta_\pi^2 \left[h_0^2(t, Q^2) - \sqrt{\frac{3}{2}} h_2^2(t, Q^2) \right] f_+^{2*}(t) \right\}, \\ -e^2 \text{Im}_t F_2(Q^2, 0, t) &= \frac{t \beta_\pi^3}{(t+Q^2)(4M_N^2-t)} \frac{5}{16} h_2^2(t, Q^2) \left[\sqrt{\frac{3}{2}} f_+^{2*}(t) - \frac{t}{4M_N} f_-^{2*}(t) \right], \end{aligned}$$

$$\begin{aligned}
-e^2 \text{Im}_t F_3(Q^2, 0, t) &= -\frac{M_N t \beta_\pi^3}{(t+Q^2)^2 (4M_N^2 - t)} \frac{5}{4} \left[h_2^2(t, Q^2) - \sqrt{\frac{2t}{Q^2}} h_1^2(t, Q^2) \right] \left[\sqrt{\frac{3}{2}} f_+^{2*}(t) - \frac{t}{4M_N} f_-^{2*}(t) \right], \\
-e^2 \text{Im}_t F_4(Q^2, 0, t) &= 0, \\
-e^2 \text{Im}_t F_5(Q^2, 0, t) &= \frac{t \beta_\pi^3}{(t+Q^2)^2} \frac{5}{32} \left[h_2^2(t, Q^2) - \sqrt{\frac{2t}{Q^2}} h_1^2(t, Q^2) \right] f_-^{2*}(t), \\
-e^2 \text{Im}_t F_6(Q^2, 0, t) &= \frac{t \beta_\pi^3}{M_N (t+Q^2)^3} \frac{5}{64} \left[\sqrt{\frac{3}{2}} Q^2 t h_0^2(t, Q^2) + \sqrt{2Q^2 t} h_1^2(t, Q^2) - \frac{Q^4 + (t+Q^2)^2}{2} h_2^2(t, Q^2) \right] f_-^{2*}(t), \\
-e^2 \text{Im}_t F_7(Q^2, 0, t) &= \frac{Q^2 t \beta_\pi^3}{(t+Q^2)^2} \frac{5}{32} \left[h_2^2(t, Q^2) - \sqrt{\frac{2t}{Q^2}} h_1^2(t, Q^2) \right] f_-^{2*}(t), \\
-e^2 \text{Im}_t F_8(Q^2, 0, t) &= -\frac{t \beta_\pi^3}{(t+Q^2)^2} \frac{5}{8} \left[h_2^2(t, Q^2) - \sqrt{\frac{2t}{Q^2}} h_1^2(t, Q^2) \right] f_-^{2*}(t), \\
-e^2 \text{Im}_t F_9(Q^2, 0, t) &= -\frac{Q^2 t \beta_\pi^3}{M_N (t+Q^2)^3} \frac{5}{32} \left[\sqrt{\frac{3}{2}} t h_0^2(t, Q^2) + \sqrt{2Q^2 t} h_1^2(t, Q^2) - \frac{Q^2}{2} h_2^2(t, Q^2) \right] f_-^{2*}(t), \\
-e^2 \text{Im}_t F_{10}(Q^2, 0, t) &= \frac{t^2 \beta_\pi^3}{(t+Q^2)^2} \frac{5}{32} \left[\sqrt{\frac{3}{2}} h_0^2(t, Q^2) - \frac{1}{2} h_2^2(t, Q^2) \right] f_-^{2*}(t), \\
-e^2 \text{Im}_t F_{11}(Q^2, 0, t) &= \frac{t^2 \beta_\pi^3}{(t+Q^2)^2} \frac{5}{128} \left[h_2^2(t, Q^2) + \sqrt{\frac{2Q^2}{t}} h_1^2(t, Q^2) \right] f_-^{2*}(t), \\
-e^2 \text{Im}_t F_{12}(Q^2, 0, t) &= -\frac{t \beta_\pi^3}{M_N (t+Q^2)^2} \frac{5}{32} \left[\sqrt{\frac{3}{2}} t h_0^2(t, Q^2) + \sqrt{2Q^2 t} h_1^2(t, Q^2) - \frac{Q^2}{2} h_2^2(t, Q^2) \right] f_-^{2*}(t). \tag{B11}
\end{aligned}$$

Note that the $\gamma\gamma^* \rightarrow \pi\pi$ partial wave helicity amplitudes are subject to kinematic constraints at the soft-photon point and at two-pion threshold [40]. For the lowest partial waves relevant here one finds

$$\begin{aligned}
h_0^0(t, Q^2) &\sim (t+Q^2), \\
h_2^2(t, Q^2) &\sim (t-4m_\pi^2)(t+Q^2), \\
h_2^2(t, Q^2) - \sqrt{\frac{2t}{Q^2}} h_1^2(t, Q^2) &\sim (t-4m_\pi^2)(t+Q^2)^2, \\
\sqrt{\frac{3}{2}} t h_0^2(t, Q^2) + \sqrt{2Q^2 t} h_1^2(t, Q^2) - \frac{Q^2}{2} h_2^2(t, Q^2) & \\
&\sim (t-4m_\pi^2)(t+Q^2)^3. \tag{B13}
\end{aligned}$$

As a consequence, in all combinations of the invariant amplitudes F_i that enter the generalized polarizabilities (see Eqs. (10)-(15)) all denominators containing powers of $(t+Q^2)$ cancel. The resulting expressions are regular at $t = -Q^2$, which provides a consistency check of our evaluation of the $\pi\pi$ contribution.

Appendix C: $\Delta(1232)$ -exchange contribution to VCS amplitudes

1. $\gamma^* N \Delta$ vertex function

To describe the $\Delta(1232)$ -exchange in the VCS process, we start from the Lagrangian describing the electromagnetic $N \rightarrow \Delta$ interaction:

$$\begin{aligned}
\mathcal{L}_{em} &= -e J_{em}^\mu A_\mu \\
&= -e \left\{ \bar{\psi}_\beta \Gamma_{\gamma N \Delta}^{\beta\mu} N + \bar{N} \tilde{\Gamma}_{\gamma N \Delta}^{\beta\mu} \psi_\beta \right\} A_\mu, \tag{C1}
\end{aligned}$$

where N is the nucleon field and ψ_β the Δ Rarita-Schwinger field. Furthermore $\Gamma_{\gamma N \Delta}^{\beta\mu}$ and $\tilde{\Gamma}_{\gamma N \Delta}^{\beta\mu}$ stand for the vertex and its adjoint, which are related by:

$$\tilde{\Gamma}_{\gamma N \Delta}^{\beta\mu} \equiv \gamma^0 \left(\Gamma_{\gamma N \Delta}^{\beta\mu} \right)^\dagger \gamma^0. \tag{C2}$$

The electromagnetic $N \rightarrow \Delta$ transition is described by three Lorentz structures corresponding with the magnetic dipole (M1), the electric quadrupole (E2), and the Coulomb quadrupole (C2) transitions. We follow the parameterization given in [55]:

$$\begin{aligned}
\Gamma_{\gamma N \Delta}^{\beta\mu}(p_\Delta, p) &= \sqrt{\frac{2}{3}} \left\{ g_M(q^2) \Gamma_M^{\beta\mu} + g_E(q^2) \Gamma_E^{\beta\mu} \right. \\
&\quad \left. + g_C(q^2) \Gamma_C^{\beta\mu} \right\}, \tag{C3}
\end{aligned}$$

with p (p_Δ) the nucleon (Δ) four-momentum respectively, with four-momentum transfer $q = p_\Delta - p$. We have defined the vertex for the $p \rightarrow \Delta^+$ transition, which yields the isospin factor $\sqrt{2/3}$. The tensors in Eq. (C3) corresponding with magnetic dipole (M), electric quadrupole (E) and Coulomb quadrupole (C) $\gamma^*N\Delta$ excitations are given by the gauge-invariant expressions:

$$\begin{aligned}\Gamma_M^{\beta\mu} &= \frac{3}{2} \frac{(M_\Delta + M_N)}{M_N Q_+^2} [i\varepsilon^{\beta\mu\kappa\lambda} (p_\Delta)_\kappa q_\lambda], \\ \Gamma_E^{\beta\mu} &= \frac{3}{2} \frac{(M_\Delta + M_N)}{M_N Q_+^2} [(q \cdot p_\Delta) g^{\beta\mu} - q^\beta (p_\Delta)^\mu] \gamma_5, \\ \Gamma_C^{\beta\mu} &= \frac{3}{2} \frac{(M_\Delta + M_N)}{M_N M_\Delta Q_+^2} [-\gamma \cdot p_\Delta (q^\beta q^\mu - q^2 g^{\beta\mu}) \\ &\quad + \gamma^\beta (q \cdot p_\Delta q^\mu - q^2 (p_\Delta)^\mu)] \gamma_5,\end{aligned}\quad (C4)$$

where

$$Q_\pm^2 \equiv (M_\Delta \pm M_N)^2 + Q^2, \quad (C5)$$

and where we adopt the convention $\varepsilon_{0123} = +1$. The vertices defined in Eq. (C4) satisfy the property:

$$(p_\Delta)_\beta \Gamma_{M,E,C}^{\beta\mu} = 0, \quad (C6)$$

which define them as "consistent" couplings [55], decoupling the unphysical spin-1/2 degrees of freedom present in the Rarita-Schwinger field. The corresponding form factors (FFs) g_M , g_E , and g_C appearing in Eq. (C3) have spacelike virtuality. It is conventional to express these FFs at the resonance position, i.e. for $p_\Delta^2 = M_\Delta^2$, in terms of the magnetic dipole (G_M^*), electric quadrupole (G_E^*), and Coulomb quadrupole (G_C^*) transition FFs as:

$$\begin{aligned}g_M &= \frac{Q_+}{M_N + M_\Delta} (G_M^* - G_E^*), \\ g_E &= -\frac{Q_+}{M_N + M_\Delta} \frac{2}{Q_-^2}\end{aligned}$$

$$\begin{aligned}g_C &= \frac{Q_+}{M_N + M_\Delta} \frac{1}{Q_-^2} \\ &\quad \times \{(M_\Delta^2 - M_N^2 - Q^2) G_E^* + Q^2 G_C^*\}, \\ &\quad \times \{4M_\Delta^2 G_E^* - (M_\Delta^2 - M_N^2 - Q^2) G_C^*\},\end{aligned}\quad (C7)$$

with the so-called Ash FFs parameterized, for spacelike virtuality $q^2 = -Q^2 < 0$, through the MAID2007 analysis [52, 56]:

$$\begin{aligned}G_M^*(Q^2) &= 3.00 (1 + 0.01 Q^2) e^{-0.23 Q^2} G_D(Q^2), \\ G_E^*(Q^2) &= 0.064 (1 - 0.021 Q^2) e^{-0.16 Q^2} G_D(Q^2), \\ G_C^*(Q^2) &= 0.124 \frac{1 + 0.12 Q^2}{1 + 4.9 \frac{Q^2}{4M_N^2}} \frac{4M_\Delta^2 e^{-0.23 Q^2}}{M_\Delta^2 - M_N^2} G_D(Q^2),\end{aligned}\quad (C8)$$

with Q^2 in GeV^2 and the dipole FF:

$$G_D(Q^2) \equiv \frac{1}{(1 + Q^2/0.71)^2}. \quad (C9)$$

2. VCS amplitudes for narrow Δ -exchange in s - and u -channel

As we are interested to model the t -channel left-hand cut for $\nu = 0$ through the Δ -exchange, we calculate the narrow $\Delta(1232)$ -exchange in s - and u -channel to the VCS amplitudes f_i in Eq. (7) that are even in ν (i.e. for $i = 1, 2, 5, 6, 7, 9, 11, 12$). For $\nu = 0$, the contribution to the odd amplitudes f_3, f_4, f_8 , and f_{10} vanishes.

As the $\gamma^*N\Delta$ transition for low Q^2 is completely dominated by the magnetic dipole excitation in Eq. (C3), we will model the left-hand cut contribution to the VCS amplitudes keeping only the magnetic dipole excitation in the $\gamma^*N\Delta$ transition. The corresponding VCS tensors $\mathcal{M}^{\mu\nu}$ of Eq. (6) due to s - and u -channel Δ -exchange are given by:

$$\mathcal{M}_{s\Delta}^{\mu\nu} = \tilde{\Gamma}_{\gamma N\Delta}^{\alpha\nu}(p', p_s) \frac{(\gamma \cdot p_s + M_\Delta)}{s - M_\Delta^2} \left[-g_{\alpha\beta} + \frac{1}{3} \gamma_\alpha \gamma_\beta \right] \Gamma_{\gamma N\Delta}^{\beta\mu}(p_s, p), \quad (C10)$$

$$\mathcal{M}_{u\Delta}^{\mu\nu} = \tilde{\Gamma}_{\gamma N\Delta}^{\alpha\mu}(p', p_u) \frac{(\gamma \cdot p_u + M_\Delta)}{u - M_\Delta^2} \left[-g_{\alpha\beta} + \frac{1}{3} \gamma_\alpha \gamma_\beta \right] \Gamma_{\gamma N\Delta}^{\beta\nu}(p_u, p), \quad (C11)$$

with $p_s = p + q$ and $p_u = p - q'$. By projecting Eqs. (C10) and (C11) on the VCS tensor basis of Eq. (7), the result-

ing expressions for the VCS amplitudes for $\nu = 0$ due to s - and u -channel Δ exchange are found as:

$$f_1^\Delta(Q^2, 0, t) = F_\Delta(Q^2, t) \left\{ -2M_N^2(M_N + M_\Delta) + \left(M_\Delta + \frac{3M_N}{4} \right) t + \frac{1}{2} \left(M_\Delta + \frac{M_N}{2} \right) Q^2 \right\}, \quad (C12)$$

$$f_2^\Delta(Q^2, 0, t) = F_\Delta(Q^2, t) \left\{ \frac{1}{2}(M_N + M_\Delta) + \frac{1}{16M_N}(t + Q^2) \right\}, \quad (\text{C13})$$

$$f_5^\Delta(Q^2, 0, t) = F_\Delta(Q^2, t) \left\{ -M_N(M_N + M_\Delta) + \frac{1}{8M_N}(M_\Delta + 7M_N)t + \frac{3}{4}Q^2 \right\}, \quad (\text{C14})$$

$$f_6^\Delta(Q^2, 0, t) = F_\Delta(Q^2, t) \left\{ \frac{1}{8}(M_N + M_\Delta) - \frac{1}{32M_N}(t + Q^2) \right\}, \quad (\text{C15})$$

$$f_7^\Delta(Q^2, 0, t) = F_\Delta(Q^2, t) \left\{ \frac{3}{4}Q^2 \right\}, \quad (\text{C16})$$

$$f_9^\Delta(Q^2, 0, t) = 0, \quad (\text{C17})$$

$$f_{11}^\Delta(Q^2, 0, t) = F_\Delta(Q^2, t) \left\{ -\frac{1}{32M_N}(M_N + M_\Delta)t - \frac{3}{16}Q^2 \right\}, \quad (\text{C18})$$

$$f_{12}^\Delta(Q^2, 0, t) = F_\Delta(Q^2, t) \left\{ \frac{1}{4}(M_N + M_\Delta) \right\}, \quad (\text{C19})$$

where we have defined the shorthand for the common prefactor:

$$F_\Delta(Q^2, t) \equiv \frac{G_M^*(0)G_M^*(Q^2)}{M_N^2 Q_+^2 (M_N^2 - \frac{1}{2}(t + Q^2) - M_\Delta^2)}. \quad (\text{C20})$$

In Ref. [57], the nucleon GPs were calculated in Baryon ChPT. As part of that calculation, also the Δ -pole contribution in the limit $t = -Q^2$ was evaluated in the δ -counting scheme. We have checked that the expressions of Eqs. (C12)-(C19) exactly agree with the expressions of Appendix B of Ref. [57] in the limit $t = -Q^2$, when making the replacement $Q_+^2 \rightarrow (M_\Delta + M_N)^2$ in Eq. (C20) to be consistent with the power counting scheme of Ref. [57].

3. $\Delta(1232)$ -resonance spectral function

The expressions of Eqs. (C12)-(C19), which have been obtained for a narrow Δ , see Eq. (C20), are of the pole form:

$$A(Q^2, t) = \frac{g(Q^2, t)}{s - M_\Delta^2}, \quad (\text{C21})$$

with $s = M_N^2 - (t + Q^2)/2$ for $\nu = 0$, and where $g(Q^2, t)$ is a smooth numerator function. The t -channel discontinuity of an amplitude of the form of Eq. (C21) for $\nu = 0$ is then obtained by the analytic continuation $t \rightarrow t + i\epsilon$ resulting in:

$$\text{Im}_t A(Q^2, t) = g(Q^2, t) [\pi\delta(s - M_\Delta^2)]. \quad (\text{C22})$$

Note the opposite sign when calculating the s - and t -channel discontinuities for $\nu = 0$.

Because in the realistic case the $\Delta(1232)$ baryon has a width of $\Gamma_\Delta = 0.117$ GeV, we next discuss the discontinuity for the case of an unstable particle. For unstable particles, the standard Cutkosky rules have to be extended by also including the resonance decay in the πN channel,

corresponding with a cut for $s \geq s_0 \equiv (M_N + m_\pi)^2$. It amounts to replace the discontinuity for the stable particle of Eq. (C22) by

$$\begin{aligned} \text{Im}_t A(Q^2, t) &= g(Q^2, t) \\ &\times \left[\pi\rho^\Delta(s = M_N^2 - \frac{1}{2}(t + Q^2); M_\Delta, \Gamma_\Delta) \right], \end{aligned} \quad (\text{C23})$$

with $\rho^\Delta(s; M_\Delta, \Gamma_\Delta)$ a spectral function, which describes the distribution of strength in the discontinuity function around the resonance position, with normalization

$$\int_{s_0}^{\infty} ds \rho^\Delta(s; M_\Delta, \Gamma_\Delta) = 1. \quad (\text{C24})$$

In the limit of a narrow resonance, the spectral function reduces to a δ -function

$$\rho^\Delta(s; M_\Delta, \Gamma_\Delta \rightarrow 0) \rightarrow \delta(s - M_\Delta^2), \quad (\text{C25})$$

resulting in Eq. (C22). For a finite width, we choose a Breit-Wigner lineshape for the spectral function

$$\rho^\Delta(s; M_\Delta, \Gamma_\Delta) = \frac{N_\Delta}{\pi} \frac{M_\Delta \Gamma_\Delta(s)}{(s - M_\Delta^2)^2 + (M_\Delta \Gamma_\Delta(s))^2}. \quad (\text{C26})$$

In the above equation, the energy dependence of the width function $\Gamma_\Delta(s)$ is given as in MAID2007 [52]

$$\begin{aligned} \Gamma_\Delta(s) &= \Gamma_\Delta \frac{|p_\pi(s)|^3}{|p_\pi(M_\Delta^2)|^3} \frac{M_\Delta}{\sqrt{s}} \\ &\times \left(\frac{|p_\pi(M_\Delta^2)|^2 + X_\Delta^2}{|p_\pi(s)|^2 + X_\Delta^2} \right) \theta(s - s_0), \end{aligned} \quad (\text{C27})$$

where the pion momentum in the πN c.m. frame is given by

$$|p_\pi(s)| = \frac{\lambda^{1/2}(s, M_N^2, m_\pi^2)}{2\sqrt{s}}, \quad (\text{C28})$$

with $\lambda(x, y, z)$ the Källén function

$$\lambda(x, y, z) \equiv x^2 + y^2 + z^2 - 2xy - 2xz - 2yz. \quad (\text{C29})$$

The $\Delta(1232)$ resonance in MAID2007 is described by the parameters

$$M_\Delta = 1.232 \text{ GeV}, \quad (\text{C30})$$

$$\Gamma_\Delta = 0.117 \text{ GeV}, \quad (\text{C31})$$

$$X_\Delta = 0.5 \text{ GeV}. \quad (\text{C32})$$

The normalization of Eq. (C24) of the spectral function implies for the normalization parameter N_Δ in Eq. (C26)

$$N_\Delta = \frac{1}{1.1567}. \quad (\text{C33})$$

-
- [1] E. Mornacchi et al. (A2 Collaboration at MAMI), *Phys. Rev. Lett.* **128**, 132503 (2022).
- [2] X. Li et al., *Phys. Rev. Lett.* **128**, 132502 (2022).
- [3] E. Mornacchi, S. Rodini, B. Pasquini, and P. Pedroni, *Phys. Rev. Lett.* **129**, 102501 (2022), 2204.13491.
- [4] D. Drechsel, B. Pasquini, and M. Vanderhaeghen, *Phys. Rept.* **378**, 99 (2003).
- [5] H. W. Griesshammer, J. A. McGovern, D. R. Phillips, and G. Feldman, *Prog. Part. Nucl. Phys.* **67**, 841 (2012).
- [6] F. Hagelstein, R. Miskimen, and V. Pascalutsa, *Prog. Part. Nucl. Phys.* **88**, 29 (2016).
- [7] B. Pasquini and M. Vanderhaeghen, *Ann. Rev. Nucl. Part. Sci.* **68**, 75 (2018).
- [8] A. Antognini, F. Hagelstein, and V. Pascalutsa, *Ann. Rev. Nucl. Part. Sci.* **72**, 389 (2022).
- [9] K. Pachucki, V. Lensky, F. Hagelstein, S. S. Li Muli, S. Bacca, and R. Pohl, *Rev. Mod. Phys.* **96**, 015001 (2024).
- [10] P. A. M. Guichon, G. Q. Liu, and A. W. Thomas, *Nucl. Phys. A* **591**, 606 (1995).
- [11] D. Drechsel, G. Knochlein, A. Y. Korchin, A. Metz, and S. Scherer, *Phys. Rev. C* **57**, 941 (1998).
- [12] M. Gorchtein, C. Lorce, B. Pasquini, and M. Vanderhaeghen, *Phys. Rev. Lett.* **104**, 112001 (2010).
- [13] J. Roche, J. M. Friedrich, D. Lhuillier, et al., *Phys. Rev. Lett.* **85**, 708 (2000).
- [14] I. K. Bensafa et al. (A1 Collaboration), *Eur. Phys. J. A* **32**, 69 (2007).
- [15] N. F. Sparveris et al., *Phys. Rev. C* **78**, 018201 (2008).
- [16] L. Doria et al. (A1 Collaboration), *Phys. Rev. C* **92**, 054307 (2015).
- [17] A. Blomberg et al., *Eur. Phys. J. A* **55**, 182 (2019).
- [18] J. Beričič, L. Correa, M. Benali, et al. (A1 Collaboration), *Phys. Rev. Lett.* **123**, 192302 (2019).
- [19] H. Fonvieille et al. (A1), *Phys. Rev. C* **103**, 025205 (2021).
- [20] P. Bourgeois et al., *Phys. Rev. Lett.* **97**, 212001 (2006).
- [21] P. Bourgeois et al., *Phys. Rev. C* **84**, 035206 (2011).
- [22] G. Laveissière et al. (Jefferson Lab Hall A Collaboration), *Phys. Rev. Lett.* **93**, 122001 (2004).
- [23] H. Fonvieille et al. (The Jefferson Lab Hall A Collaboration), *Phys. Rev. C* **86**, 015210 (2012).
- [24] R. Li et al., *Nature* **611**, 265 (2022).
- [25] P. A. M. Guichon and M. Vanderhaeghen, *Prog. Part. Nucl. Phys.* **41**, 125 (1998).
- [26] H. Fonvieille, B. Pasquini, and N. Sparveris, *Prog. Part. Nucl. Phys.* **113**, 103754 (2020).
- [27] M. Gell-Mann, M. L. Goldberger, and W. E. Thirring, *Phys. Rev.* **95**, 1612 (1954).
- [28] M. L. Goldberger, *Phys. Rev.* **97**, 508 (1955).
- [29] M. Gell-Mann and M. L. Goldberger, *Phys. Rev.* **96**, 1433 (1954).
- [30] F. E. Low, *Phys. Rev.* **96**, 1428 (1954).
- [31] A. I. L'vov, V. A. Petrun'kin, and M. Schumacher, *Phys. Rev. C* **55**, 359 (1997).
- [32] D. Drechsel, M. Gorchtein, B. Pasquini, and M. Vanderhaeghen, *Phys. Rev. C* **61**, 015204 (1999).
- [33] B. Pasquini, D. Drechsel, and M. Vanderhaeghen, *Phys. Rev. C* **76**, 015203 (2007).
- [34] B. Pasquini, D. Drechsel, M. Gorchtein, A. Metz, and M. Vanderhaeghen, *Phys. Rev. C* **62**, 052201 (2000).
- [35] B. Pasquini, M. Gorchtein, D. Drechsel, A. Metz, and M. Vanderhaeghen, *Eur. Phys. J. A* **11**, 185 (2001).
- [36] G. Höhler, in *Landolt-Börnstein-Group I Elementary Particles, Nuclei and Atoms, Vol. I/9b2*, edited by H. Schopper (Springer, Berlin, Heidelberg, 1983).
- [37] R. Garcia-Martin and B. Moussallam, *Eur. Phys. J. C* **70**, 155 (2010), 1006.5373.
- [38] B. Moussallam, *Eur. Phys. J. C* **73**, 2539 (2013), 1305.3143.
- [39] G. Colangelo, M. Hoferichter, M. Procura, and P. Stoffer, *JHEP* **04**, 161 (2017).
- [40] I. Danilkin and M. Vanderhaeghen, *Phys. Lett. B* **789**, 366 (2019).
- [41] M. Hoferichter and P. Stoffer, *JHEP* **07**, 073 (2019).
- [42] I. Danilkin, O. Deineka, and M. Vanderhaeghen, *Phys. Rev. D* **101**, 054008 (2020).
- [43] M. Hoferichter, J. Ruiz de Elvira, B. Kubis, and U.-G. Meißner, *Phys. Rept.* **625**, 1 (2016).
- [44] H. Atac et al., JLab VCS-II Experiment E12-23-001 (2023), 2308.07197.
- [45] N. Sparveris et al., JLab Experiment E12-25-008 (2025).
- [46] R. Tarrach, *Nuovo Cim. A* **28**, 409 (1975).
- [47] D. Drechsel, G. Knochlein, A. Y. Korchin, A. Metz, and S. Scherer, *Phys. Rev. C* **58**, 1751 (1998).
- [48] I. Danilkin, C. F. Redmer, and M. Vanderhaeghen, *Prog. Part. Nucl. Phys.* **107**, 20 (2019).
- [49] I. Caprini, G. Colangelo, and H. Leutwyler, *Eur. Phys. J. C* **72**, 1860 (2012), 1111.7160.
- [50] R. Garcia-Martin, R. Kaminski, J. R. Pelaez, J. Ruiz de Elvira, and F. J. Yndurain, *Phys. Rev. D* **83**, 074004 (2011), 1102.2183.
- [51] W. R. Frazer and J. R. Fulco, *Phys. Rev.* **117**, 1609 (1960).
- [52] D. Drechsel, S. Kamalov, and L. Tiator, *Eur. Phys. J. A* **34**, 69 (2007).
- [53] J. C. Bernauer et al. (A1), *Phys. Rev. Lett.* **105**, 242001 (2010).
- [54] M. Vanderhaeghen, *Phys. Lett. B* **402**, 243 (1997).
- [55] V. Pascalutsa, M. Vanderhaeghen, and S. N. Yang, *Phys.*

Rept. **437**, 125 (2007).

- [56] L. Tiator, D. Drechsel, S. Kamalov, and M. Vanderhaeghen, Eur. Phys. J. ST **198**, 141 (2011).
- [57] V. Lensky, V. Pascalutsa, and M. Vanderhaeghen, Eur. Phys. J. C **77**, 119 (2017).